Technical Report GL-94-11
April 1994

US Army Corps
of Engineers
Waterways Experiment
Station

Detemination of Soil Moduli in Soil-Structure Systems on Highways

Report 1
Surface Waves in Sloping Ground

by David W. Sykora, Don R. Alexander

Jose M. Roesset
University of Texas at Austin

Prepared for Headquarters, U.S. Army Corps of Engineers

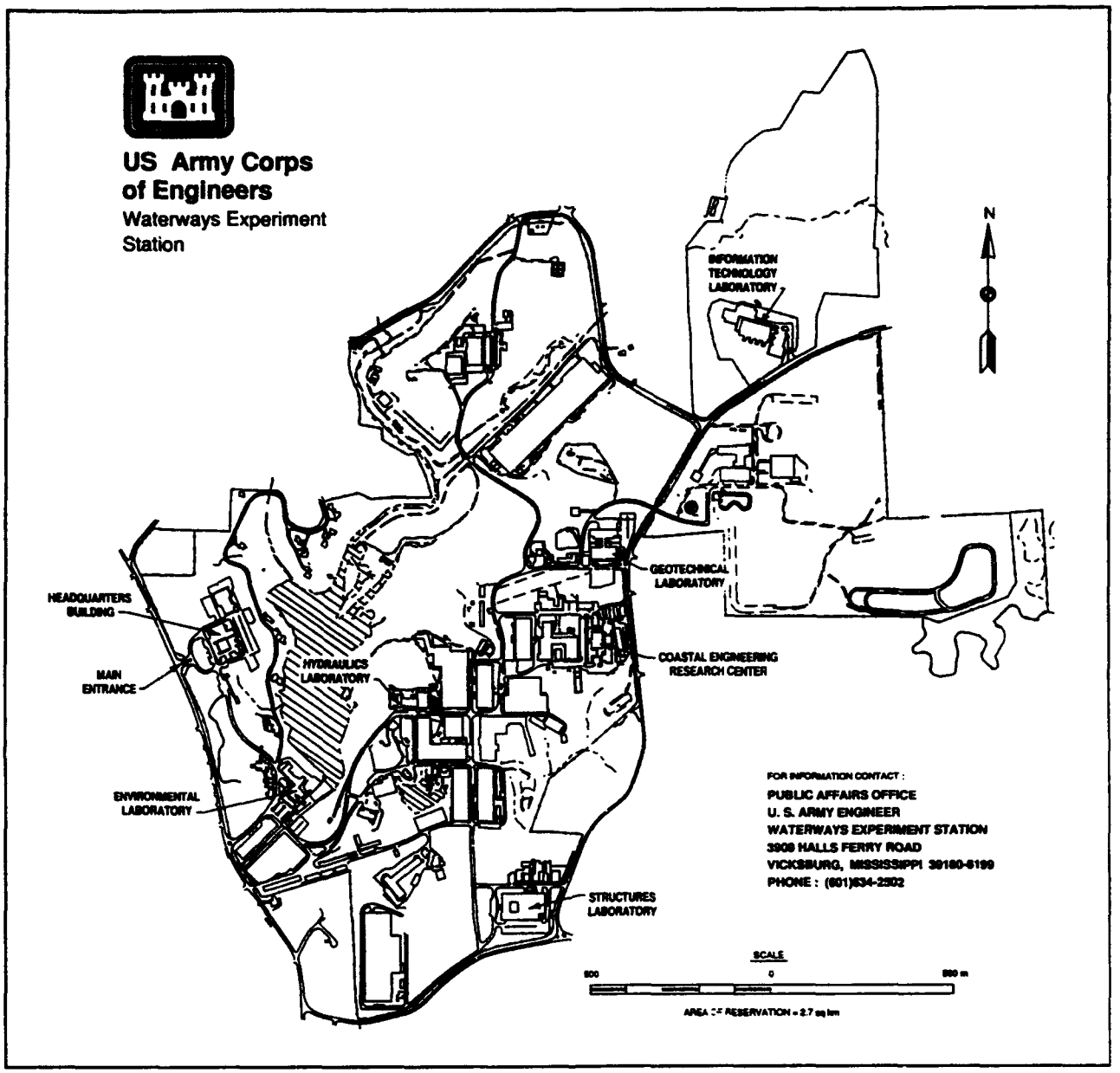

Waterways Experiment Station Cataloging-in-Publication Data

Sykora, David W.
Determination of soil moduli in soil-structure systems on highways. Report 1, Surface waves in sloping ground / by David W. Sykora, Don R. Alexander, Jose M. Roesset ; prepared for U.S. Army Corps of Engineers.
64 p. : ill. ; 28 cm. — (Technical report ; GL-94-11 rept. 1)
Includes bibliographic references.
1. Surface waves — Measurement. 2. Slopes (Soil mechanics) 3. Soil structure. 4. SASW (Computer program) I. Alexander, Don R. II. Roesset, Jose M. III. United States. Army. Corps of Engineers. IV. U.S. Army Engineer Waterways Experiment Station. V. Title. VI. Title: Surface waves in sloping ground. VIII. Series: Technical report (U.S. Army Engineer Waterways Experiment Station) ; GL-94-11 rept. 1.
TA7 W34 no.GL-94-11 rept. 1

Technical Report GL-94-11
April 1994

Determination of Soil Moduli in Soil-Structure Systems on Highways

Report 1
Surface Waves Sloping Ground

by David W. Sykora, Don R. Alexander

U.S. Army Corps of Engineers
Waterways Experiment Station
3909 Halls Ferry Road
Vicksburg, MS 39180-6199

Jose M. Roesset

University of Texas at Austin
Austin, TX 78712

Report 1 of a Series

Prepared for U.S. Army Corps of Engineers
Washington, DC 20314-1000

Contents

List of Figures

Preface

This report documents research conducted by the U.S. Army Engineer Waterways Experiment Station (WES) for the Federal Highway Administration, Turner-Fairbank Highway Research Center, Washington, D.C., through Agreement No. DTFH61-93-Y-00012 during the period 1 June 1993 through 1 June 1994. Mr. Carl Ealy (HNR-30) was the Technical Monitor.

The WES Principal Investigator was Dr. David W. Sykora, Earthquake Engineering and Seismology Branch (EESB), Earthquake Engineering and Geosciences Division (EEGD), Geotechnical Laboratory (GL), WES. Professor Jose Roesset, Department of Civil Engineering, University of Texas at Austin, guided the analytical portions of the study. Mr. Don R. Alexander, Criteria Development and Applications Branch (CDAB), Pavement Systems Division (PSD), GL, WES, conducted field measurements and assisted in data processing. Messrs. Leo Koestler and Roger Meier, WES, and Prof. Glenn Rix, Georgia Institute of Technology, assisted in field measurements at the WES test site. Ms. Jennifer J. Davis-Smith, a co-op student from Mississippi State University, helped to prepare report figures. Dr. Mary Ellen Hynes was the Chief, EESB, and Dr. Albert J. Bush III was the Chief, CDAB, during the study.

Overall direction at WES was provided by Dr. A. G. Franklin, Chief, EEGD, Dr. George M. Hammitt II, Chief, PSD, and Dr. William F. Marcuson III, Director, GL.

At the time of publication of this report, Director of WES was Dr. Robert W. Whalin. Commander was COL Bruce K. Howard, EN.

1 Introduction

Federal and state highway officials are finding through experience that existing design codes (e.g., Applied Technology Council 1981 and 1983; American Association of State Highway and Transportation Officials 1991) may be inadequate to mitigate damage produced to bridges by moderate to large earthquakes especially at soft soil sites (Miranda 1993). A number of different research and development efforts are underway at various institutions to examine this problem. One such research program administered by the Federal Highway Administration (FHWA), is aimed at geotechnical aspects of seismic design for bridge abutments, embankments, and foundations.

Paramount to calculating the seismic behavior of a bridge are the earthquake motions at the foundations. Seismic forces are applied at the abutments and at piers along the length of the deck. The soil conditions at each foundation are likely to be significantly different, however, possibly varying from rock to soft soil to rock and almost always varying in thickness of soil below the abutment or thickness of soil below a pier. Wave passage effects and asynchronous motion may also impact the selection of appropriate seismic motions. Combinations of these factors may produce a large variation in seismic inputs over the length of the bridge.

Traditional solutions involving equally-distributed seismic forces appear to be in question and more comprehensive dynamic response analyses of the complete bridge-foundation system or individual foundation systems are being considered. The more comprehensive analyses allow for variations in foundation and soil conditions and earthquake wave directivity. Hence, a thorough understanding of how to adequately characterize and idealize soil stiffness (elastic moduli) in the vicinity of the bridge foundations and within embankments is warranted.

Extensive research and development of seismic methods to determine elastic moduli has occurred over the past decade. These methods include the downhole, uphole, crosshole, and the Spectral-Analysis-of-Surface-Waves (SASW) methods. Data collection and processing for nearly all of these methods were developed under the assumption that the ground is level and the sub-surface layers are horizontal and extend to infinity. These assumptions generally do not apply to bridge abutments which are typically placed at the crest of a sloping (approach) embankment fill or a cut slope.

The overall research program, entitled "In-Situ Determination of Dynamic Soil Properties for Highway Structures," is intended to carefully examine the effects of complex geosystems (soil-rock systems) and anisotropic states of stress on existing seismic methods. The efforts will include numerical analysis, laboratory testing, and field measurements using existing techniques and possible modifications.

The seismic methods to be considered as part of the program are: downhole, crosshole, SASW, and seismic tomography. This report (Report 1 of a series) specifically summarizes the analysis of the vertical component of surface waves in sloping ground using numerical analysis and field measurements. Once each method has been re-evaluated, a procedure for applying various seismic geophysical methods to the characterization and idealization of complex soil-rock systems will be developed.

The SASW method offers a unique and economical alternative means for the determination of stiffness for near-surface conditions. One simplifying assumption made for inversion schemes of the SASW method is that the ground is level which not only precludes the existence of discontinuities, but also implies that the state of stress is isotropic. The presence of a slope defies this assumption. Therefore, surface waves propagating up, down, and along a slope were evaluated using the results of numerical approximations and field measurements to assess the effects of sloping ground.

To begin, the SASW method is described in Chapter 2 of this report. A brief description of the numerical analysis procedures and validation of the computer code used are presented in Chapter 3. The results of the numerical analysis which considers several different slope angles and set-back distances are described in Chapter 4. Field measurements conducted at a test site at WES are described and compared with numerical results in Chapter 5.

2 The SASW Method

The analysis of surface waves has been used for several decades to obtain the variation of soil stiffness with depth. The steady-state surface wave technique was developed in the late 1950's (Heukelom 1958; Jones 1958; Heukelom and Foster 1960) for the analysis of pavement systems. This technology was adapted by WES to be an exploration tool at soil sites (Fry 1963 and 1965; Ballard 1964). This technique involves interactively determining the wavelength at several frequencies of excitation by measuring the distances from the source to successive standing wave (displacement) peaks. The velocity calculated knowing the wavelength, λ, and frequency of excitation, f:

$$V_R = f\lambda \tag{2.1}$$

was assumed to correspond to the Rayleigh wave velocity, V_R, at an average depth between $\lambda/3$ and $\lambda/2$.

The SASW method was developed nearly two decades later (Heisey 1982; Heisey, Stokoe, and Meyer 1982; Nazarian 1984; and Nazarian and Stokoe 1985a, 1985b) under the direction of Professor Stokoe at the University of Texas at Austin (UT). Since that time, research, development, and application activities have continued at UT under the tutelage of Professors Stokoe and Roesset (e.g., Calderon 1985; Nogueira 1986; Sanchez-Salinero 1987; Sheu 1987; Rix 1988; Kang 1990; Sykora 1993), at the University of Michigan (e.g., Hiltunen 1988; and Gucunski 1991), and at WES (Alexander 1992).

The SASW method was established to obtain a more accurate variation of elastic moduli with depth. The procedure involves measuring seismic signals at the ground surface (thus it is non-intrusive) produced by either a harmonic or impulsive surface excitation. In the original inversion schemes, the site was assumed to be ideally layered (horizontal and extending to infinity) and only plane waves were assumed to propagate. Newer inversion schemes developed at UT also provide for the effect of three-dimensional wave fronts. The determination of a stiffness profile using the SASW method consists of three phases: data measurement, signal analysis, and inversion, each of which is described briefly below.

Data Measurement

Signals typically are recorded from two sensors as shown in Figure 1 and stored digitally. The sensors may be velocity or acceleration transducers; acceleration transducers are normally reserved for cases when a significant amount of high frequency energy is being recorded. If the source is impulsive (Figure 1a), a time window with the full length of the transient response is collected as shown in Figure 2. If the source is harmonic (Figure 1b), the cross-power spectrum phase difference and coherence between the source and each receiver are calculated directly using a dynamic signal analyzer, averaged with a number of other responses using the same configuration and source, and stored as shown in Figure 3. The signal for the source is taken directly from the signal generator function on the analyzer.

The most common procedure for measurement is to keep the two receivers separated (in-line) by the same distance that the first receiver is from the source (common midpoint method) as depicted in Figure 4. Guidelines for relationships between receiver spacing and predominant wavelengths (function of f) have been proposed. Heisey (1982) suggested that the receiver spacing, d ($= d_2 - d_1$), be limited to the range:

$$\frac{\lambda}{3} \leq d \leq 2\lambda \tag{2.2}$$

An analytical study by Sanchez-Salinero (1987) suggested that d_2/d_1 be large (e.g., $d_2/d_1 \geq 4$). However, if $d_2/d_1 = 2$, then the wavelengths considered should be limited to:

$$\lambda < d_1 \tag{2.3}$$

The results from semi-analytical studies by Sykora (1993) agree with the work by Sanchez-Salinero. However, from a practical standpoint for surface waves in pavement systems, Rix (1988) suggests that the range of acceptable spacings be widened to:

$$\frac{\lambda}{3} \leq d \leq 3\lambda \tag{2.4}$$

Signal Analysis

Signal analysis is normally performed using hardware provided with the spectral analyzer. Data for harmonic sources are immediately converted to cross-power phase and coherence and averaged as described in the previous section. For impulsive sources, the time records of displacement are first

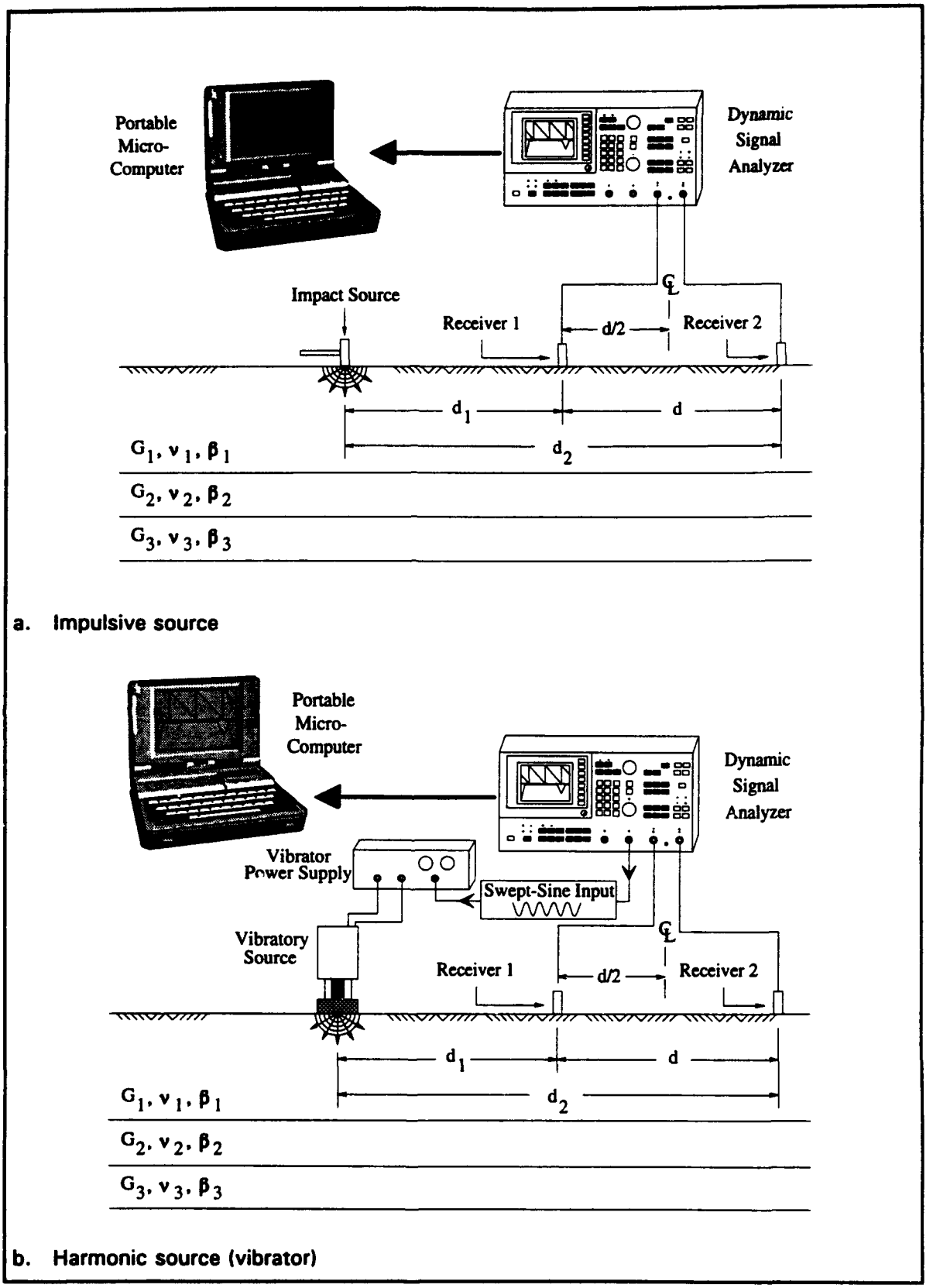

Figure 1. Schematic of SASW method (adapted from Nazarian and Stokoe 1986)

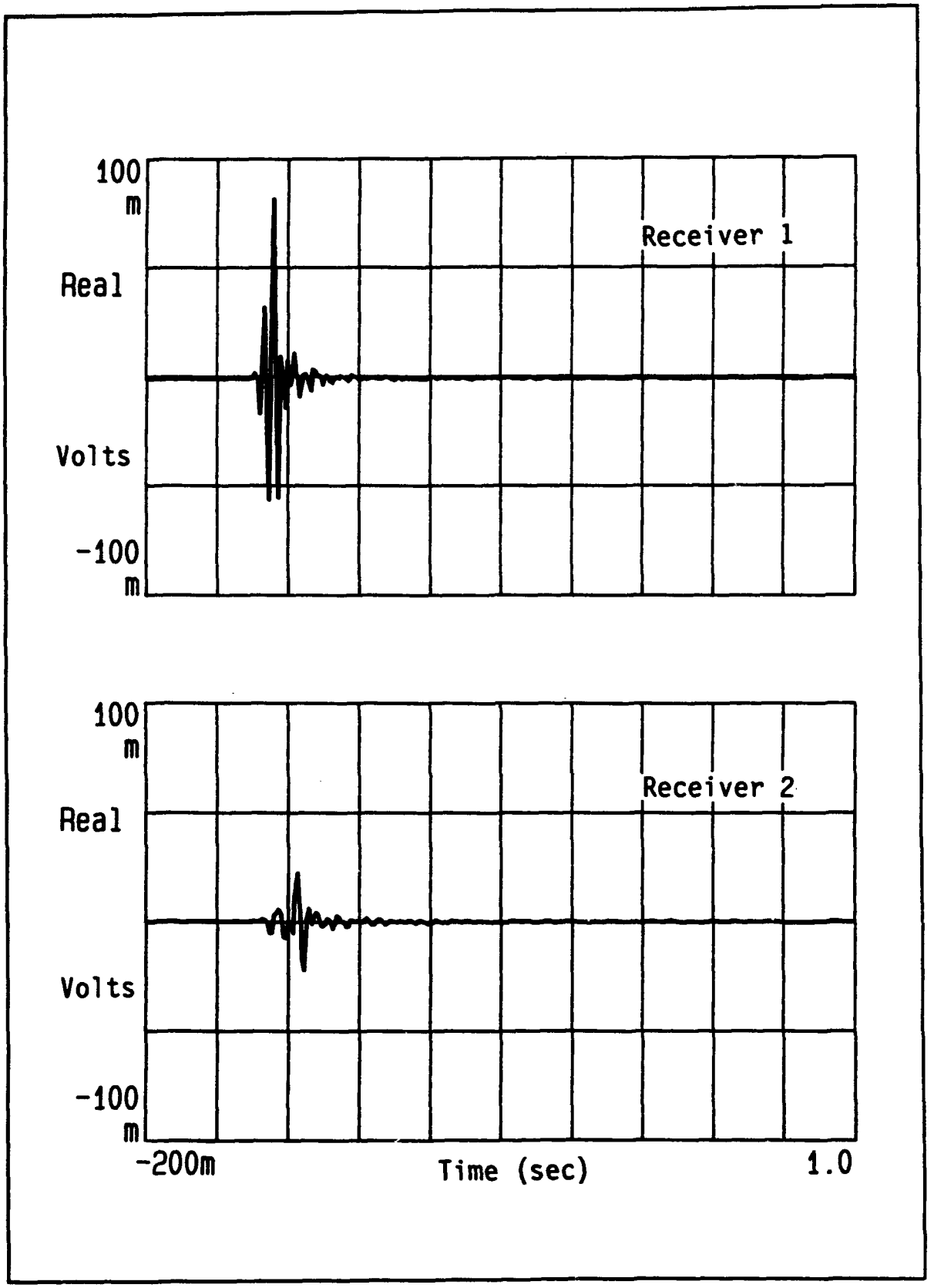

Figure 2. Impulsive signature produced by hammer striking level ground at receiver spacing of 16 ft

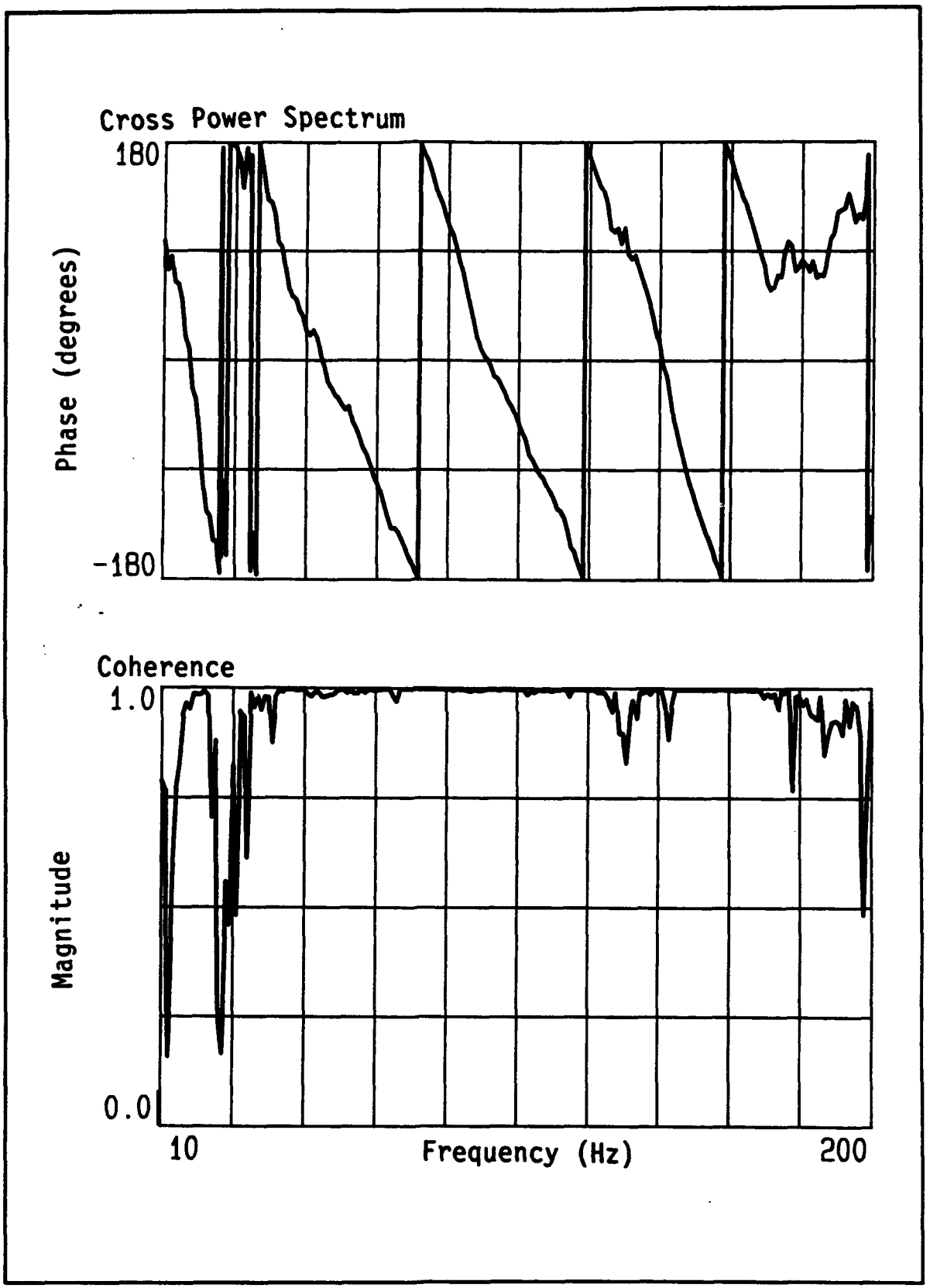

Figure 3. Phase of cross-power spectrum and magnitude of coherence produced by vibrator on level ground at receiver spacing of 8 ft

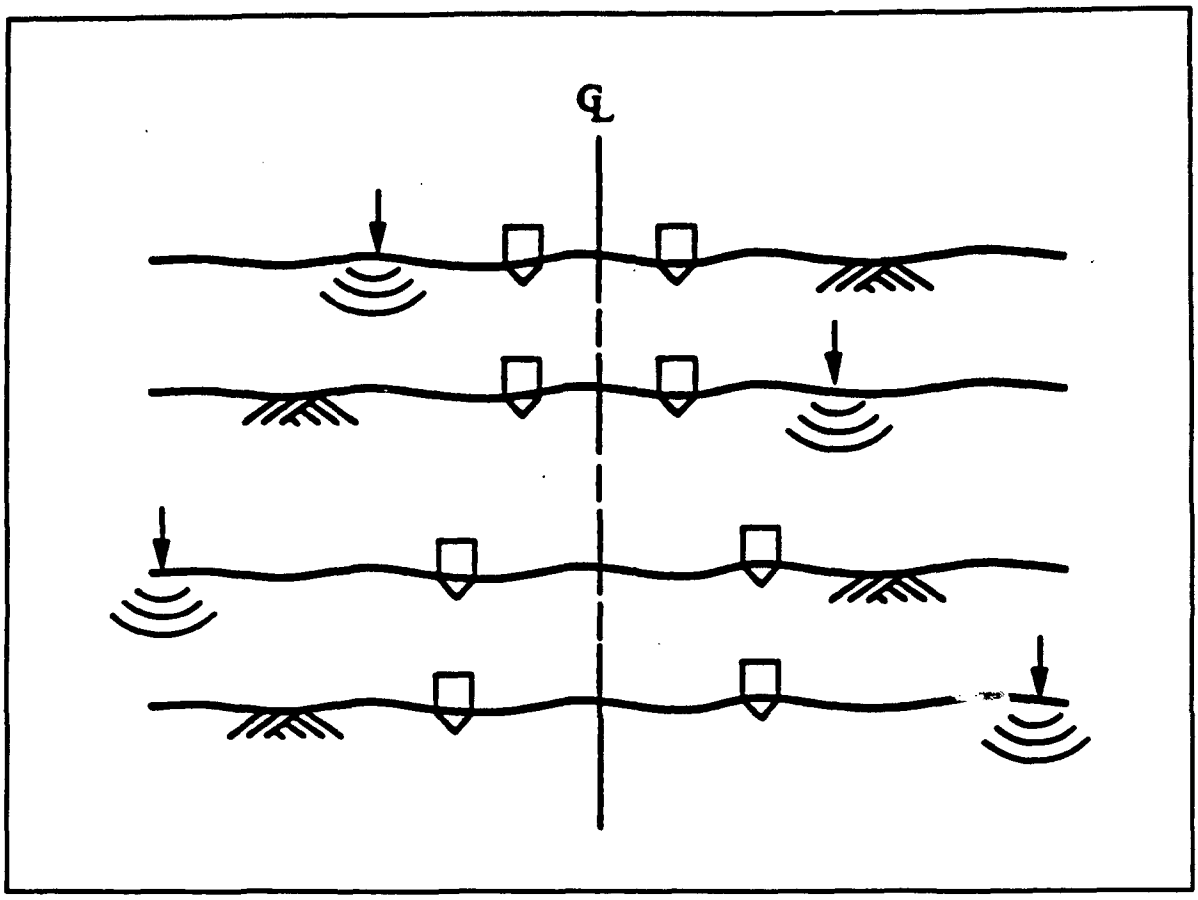

Figure 4. Arrangement of source and receiver illustrating the common receiver midpoint geometry (Rix 1988)

averaged, then the data analyzed to determine the variation of signal phase as a function of source frequency and develop a dispersion curve (variation of phase velocity versus wavelength).

The phase velocity and wavelength are calculated directly from the real and imaginary parts of the dynamic displacements (Nazarian and Stokoe 1985a). At a given frequency, f, the travel time, t, between two receivers is:

$$t = \frac{\phi_2 - \phi_1}{360\, f} \tag{2.5}$$

where ϕ_1 and ϕ_2 are the phases at points 1 and 2 (the location of the receivers) in degrees as shown in Figure 5. Then, the phase velocity, C_ϕ, is:

$$C_\phi = \frac{(d_2 - d_1)}{t} = 360\, f \frac{(d_2 - d_1)}{(\phi_2 - \phi_1)} \tag{2.6}$$

where the wavelength, λ, is:

$$\lambda = \frac{C_\phi}{f} \qquad (2.7)$$

An example of the calculation procedure is also presented in Figure 5.

Inversion

Inversion presently is an iterative process which is independent of whether the data were collected using an impulsive or a harmonic source. This step involves selecting an initial profile of layer thicknesses and moduli, calculating the dispersion curve using matrix solutions (Haskell 1953 and Thompson 1950), comparing the measured and matrix-calculated dispersion curves, modifying the profile if necessary, then repeating the process until a close match exists. A flowchart of this process is shown in Figure 6. The inverse problem does not necessarily produce a unique solution. Automatic matrix inversion using least squares is used at UT and elsewhere (Nazarian and Desai 1993) and neural networks (Rix and Leipski 1991) have been proposed as an alternative to the original matrix scheme.

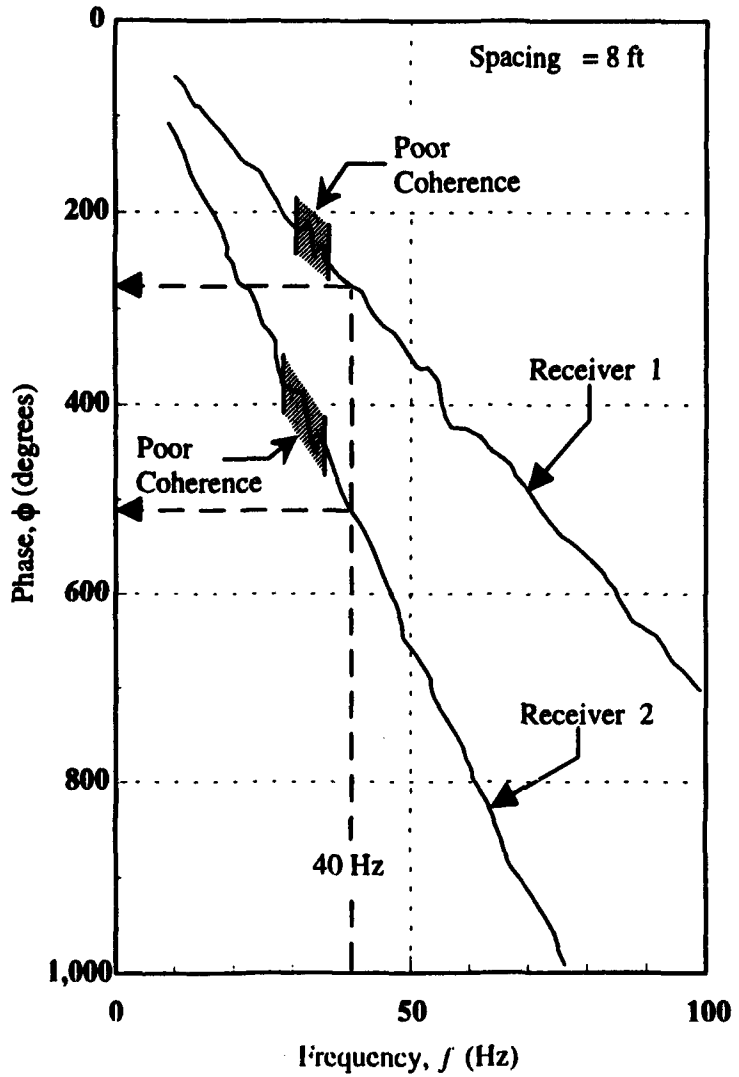

Given:

$d = d_2 - d_1 = 8$ ft

$f = 40$ Hz

Solution:

$\phi_1 = 284$ deg

$\phi_2 = 512$ deg

Phase Velocity

$$C_\phi = 360\ (f)\frac{d}{\phi_2 - \phi_1}$$

$$= \frac{360\ (40)\ (8)}{228} = \underline{505\ \text{ft/sec}}$$

Wavelength

$$\lambda = \frac{C_\phi}{f} = \frac{505}{40} = \underline{12.6\ \text{ft}}$$

Figure 5. Example of calculating phase velocity from unwrapped phase

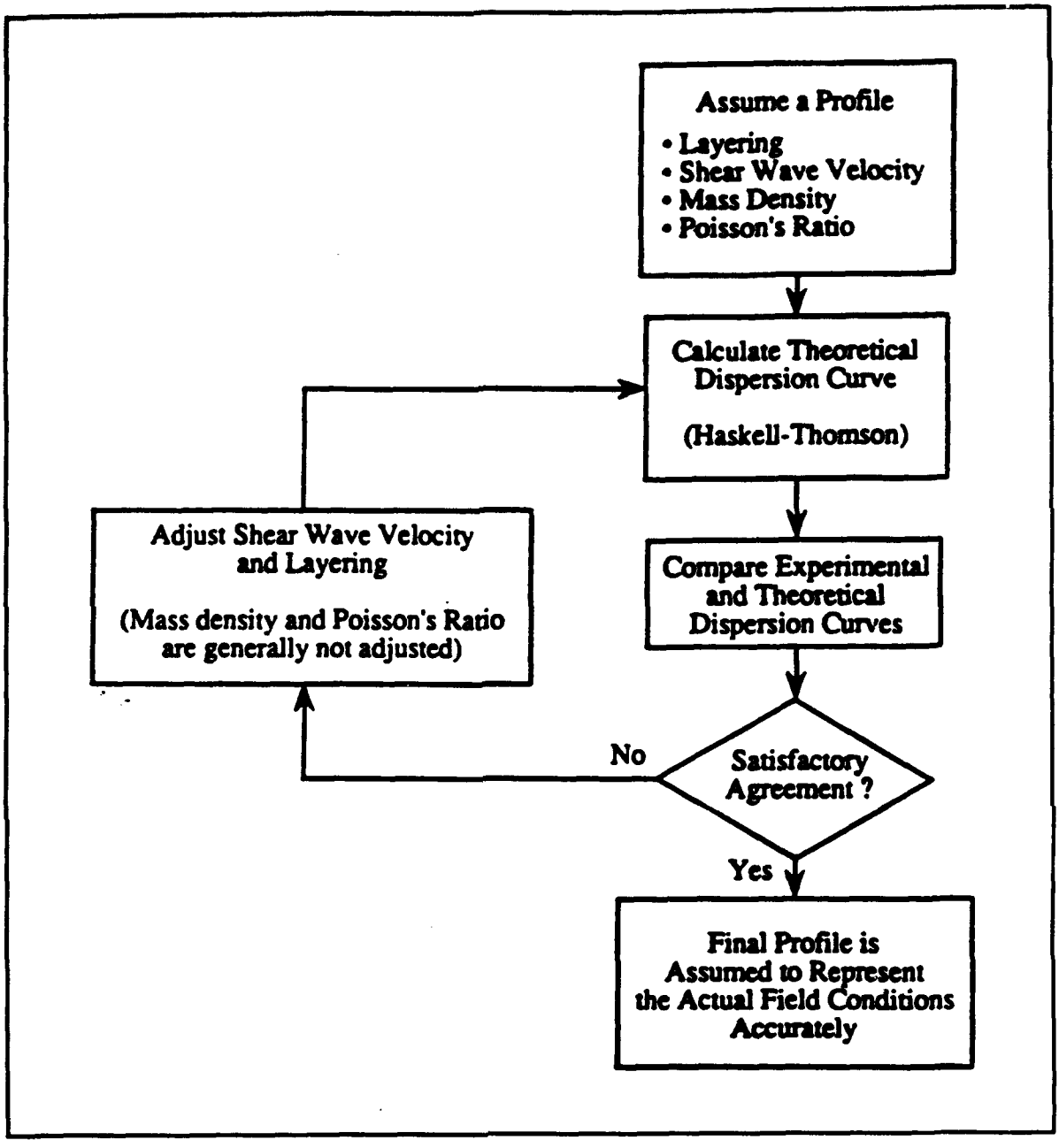

Figure 6. Flow chart summarizing the inversion procedure (Rix 1988)

3 Numerical Approximation Method

The computer code *vib3* is a research tool developed at WES to numerically approximate surface wave propagation in complex geosystems, including sloping ground. This code was created using principles of the Finite Element Method (FEM) and written using the Fortran 77 language running on U.S. Army and Department of Defense CRAY supercomputers at WES (Sykora and Roesset 1992; Sykora 1993). It has been validated with closed-form solutions for axi-symmetric problems. Parametric analysis have also been conducted to define appropriate ranges for system and problem variables. Another type of problem examined and reported elsewhere (Sykora 1993) is buried layers, both continuous and discontinuous. Salient aspects of the computer code are presented below.

Formulation and Implementation

The primary assumptions used to develop *vib3* are that the geometry and boundary conditions of the system and the distribution of material properties are planar (2-D) but the loads can be non-planar (3-D). This set of conditions has a broader range of applications than that for plane strain (commonly used in engineering analysis) while circumventing expensive 3-D solution methods. The other assumptions are:

a. All media are isotropic,

b. The hysteretic behavior is represented by complex moduli,

c. The source produces vertical, steady-state excitation on the ground surface at one discrete frequency, and

d. The distribution of loads is symmetric in the out-of-plane direction about the analysis plane.

Only fixed and free boundary conditions were used for this study. Fixed conditions were used for the base and free conditions were used elsewhere. Boundaries were placed sufficiently far from the source and points of interest

to avoid the effects of any reflections. The distances to boundaries were selected based on parametric analysis of boundary locations.

The formulation involves two primary components: the condensation of 3-D dynamic stiffness matrices to equivalent 2-D matrices and the representation of the distribution of loads in the out-of-plane direction using a Fourier expansion. The 2-D system of equations are first solved in the frequency and wave-number domain; inverse Fourier transforms are then performed to obtain the solution as a function of out-of-plane distance and time, if so desired.

The FEM is a numerical analysis technique used to approximate the response of a continuous body by dividing the domain of interest into a discrete number of subdomains. Boundary conditions and external forces are imposed at discrete nodes where the displacements are calculated. Results can be interpolated at any point in the body through the use of interpolation functions. In general, as the subdomains become smaller, the solution converges to that of the continuum.

The basic equations describing a steady-state system using a displacement formulation are:

$$(\mathbf{K} - \omega^2 \mathbf{M})\, \bar{\mathbf{U}} = \bar{\mathbf{P}} \tag{3.1}$$

where

$\mathbf{K}$ = "static" stiffness matrix
ω = circular frequency (rad/sec)
$\underline{\mathbf{M}}$ = lumped mass matrix
$\underline{\mathbf{U}}$ = vector of displacements
$\mathbf{P}$ = vector of forces

Calling $\bar{\mathbf{S}}$ the dynamic stiffness matrix defined by:

$$\bar{\mathbf{S}} = \mathbf{K} - \omega^2 \mathbf{M} \tag{3.2}$$

then

$$\bar{\mathbf{S}}\, \bar{\mathbf{U}} = \bar{\mathbf{P}} \tag{3.3}$$

Modification to constitutive model

Soil is an inelastic material—energy dissipates from friction between particles as waves travel through it. This loss of energy is represented through the use of material damping. Different mathematical models are used to approximate damping in the governing equations. One form, called hysteretic damping, is frequency independent. This form of damping can be introduced into

the formulation for frequency-domain analyses through the Correspondence Principle (Wolf 1985). This principle states that the elastic stiffness (in this case shear modulus, G) is replaced by a complex stiffness to obtain the damped solution. The following relationship is commonly used to model linear-hysteretic behavior for small shear strains (and small values of damping):

$$G^* = G\,(1 + 2i\beta) \tag{3.4}$$

where

G^* = complex shear modulus
β = damping ratio
$i = \sqrt{-1}$

The results of this study are expected to be applied at distances greater than one wavelength from the source where shear strains are small for synthetic sources. The magnitude of damping is considered to be independent of strain (Hardin and Drnevich 1972; Johnston, Toksoz, and Timur 1979; and Toksoz, Johnston, Timur 1979) for the levels of shear strains expected.

Fourier superposition

Fourier superposition is a three-step solution process for linear systems that involves a forward transformation into a wavenumber domain (either spatial or temporal), the calculation of a solution vector of displacements (Eq. 3.3) at a number of increments, and the determination of the total solution through an inverse transformation of all incremental solutions. Fourier superposition applied in both the time and y-spatial domains leads to the transform pair:

$$\bar{p}(m,\omega) = \int_{-\infty}^{+\infty} \int_{-\infty}^{+\infty} p(y,t)\, e^{-i(\omega t - my)}\, dt\, dy \tag{3.5}$$

$$p(y,t) = \frac{1}{4\pi^2} \int_{-\infty}^{+\infty} \int_{-\infty}^{+\infty} \bar{p}(m,\omega)\, e^{i(\omega t - my)}\, d\omega\, dm \tag{3.6}$$

where

p = distribution of forces with respect to y-direction and time
$\bar{p}$ = distribution of forces in wavenumber domain
m = wavenumber (spatial circular frequency) in y-direction

Making the load vector specific to steady-state vibrations with constant amplitude, then:

$$\bar{p}(m)_\omega = \int_{-\infty}^{+\infty} \bar{p}(y)\, e^{imy}\, dy \tag{3.7}$$

$$p(y,t) = \frac{e^{i\omega t}}{2\pi} \int_{-\infty}^{+\infty} \bar{p}(m)_\omega\, e^{-imy}\, dm \tag{3.8}$$

for a specific ω. The corresponding equations for displacements are:

$$\bar{u}(m)_\omega = \int_{-\infty}^{+\infty} u(y)\, e^{imy}\, dy \tag{3.9}$$

$$u(y,t) = \frac{e^{i\omega t}}{2\pi} \int_{-\infty}^{+\infty} \bar{u}(m)_\omega\, e^{-imy}\, dm \tag{3.10}$$

where

u = distribution of displacements with respect to y-direction
$\bar{u}$ = distribution of displacements in wavenumber domain

Element condensation

The process of element condensation is the key aspect of the reduction of computational effort. Element condensation refers to the process of reducing the number of degrees of freedom by relating points adjacent in the y-direction using the functional relationship of the Fourier expansion. The dependent degrees of freedom are then eliminated by expressing them in terms of the in-plane degrees of freedom.

Finite element condensation has been used successfully by a number of previous investigators. This strategy was explicitly proposed for axi-symmetric problems by Winnicki and Zienkiewicz (1979) and Lai and Booker (1991) and for 3-D formulations by Runesson and Booker (1982, 1983) and Lin and Tassoulas (1987). Element condensation was reported by Kang (1990) and Hanazato et al. (1991) for wave propagation studies in horizontally layered pavement systems. For this study, the degrees of freedom corresponding to the nodes outside of the x-z plane are eliminated. Each node in the two-dimensional mesh maintains three degrees of freedom.

Consider an arbitrary discretized model of a slope system that meets the requirement of uniform geometry and material properties in one direction such as that shown in Figure 7. The coordinate system is chosen to have the z-direction positive down and the other in-plane direction to be x. Consider three vertical planes separated by a distance of Δy at some arbitrary location along the geosystem. The dynamic stiffness matrix for a single element between two slices can be partitioned as:

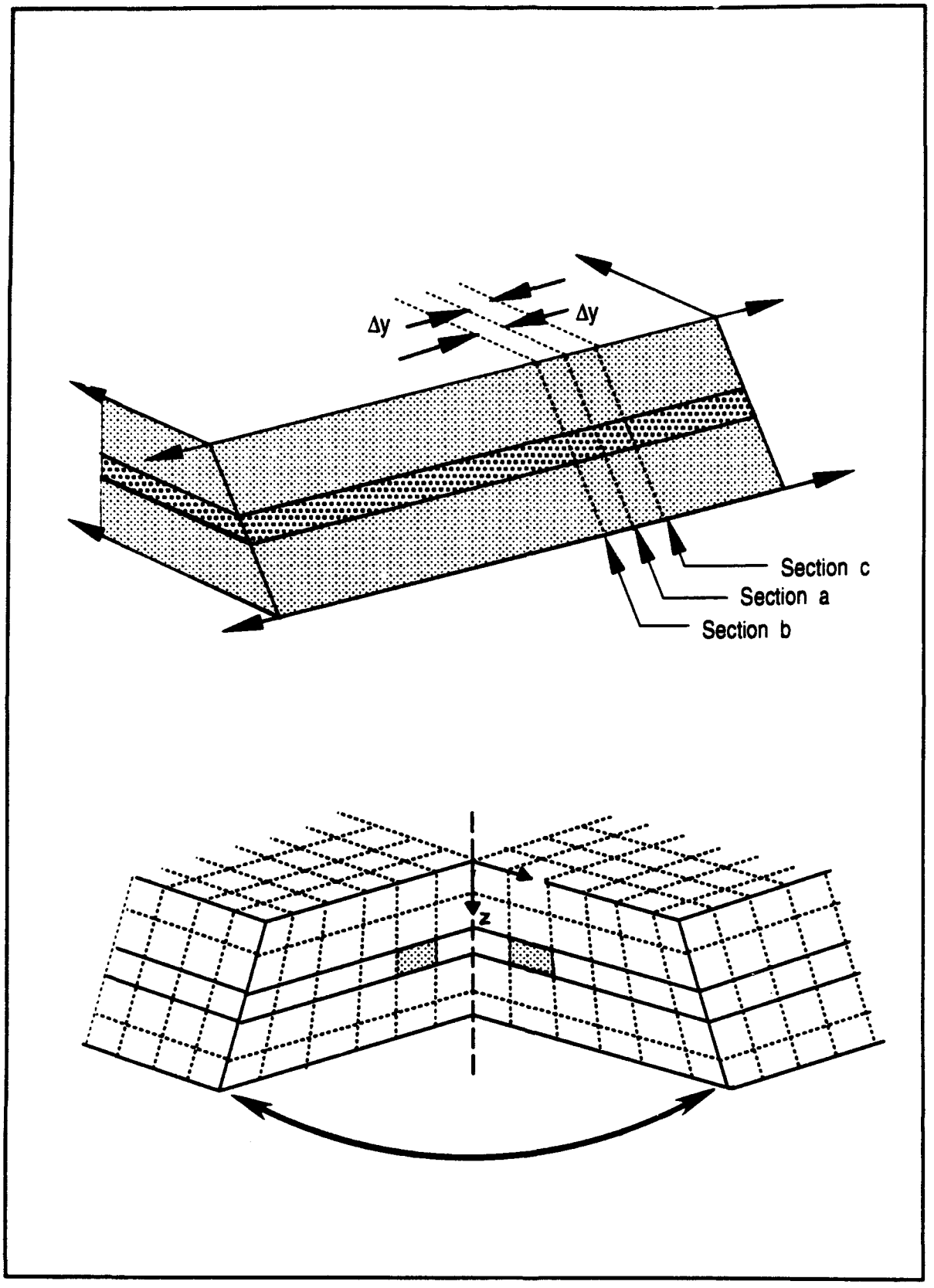

Figure 7. Example of a physical system for purposes of extracting a slice of finite elements

$$\bar{S} = \begin{bmatrix} \bar{s}_{11} & \bar{s}_{12} \\ \bar{s}_{21} & \bar{s}_{22} \end{bmatrix} \tag{3.11}$$

where the subscripts "1" and "2" refer to the degrees of freedom on the positive and negative face in the y-direction, respectively. The assemblage of the dynamic equations for any two finite elements adjacent in the y-direction, as shown in Figure 8b, can be reduced by canceling the time-dependent exponential term on each side to:

$$\begin{bmatrix} \bar{s}_{11}^{+} & \bar{s}_{12}^{+} & 0 \\ \bar{s}_{21}^{+} & \bar{s}_{22}^{+}+\bar{s}_{11}^{-} & \bar{s}_{12}^{-} \\ 0 & \bar{s}_{21}^{-} & \bar{s}_{22}^{-} \end{bmatrix} \begin{Bmatrix} \bar{U}_b \\ \bar{U}_a \\ \bar{U}_c \end{Bmatrix} = \begin{Bmatrix} \bar{P}_b \\ \bar{P}_a \\ \bar{P}_c \end{Bmatrix} \tag{3.12}$$

where

$\bar{U}$ = 2-D vector of displacements on designated face
$\bar{P}$ = 2-D vector of forces acting on designated face
"+" denotes element in + y-direction (from Δy to 0)
"-" denotes element in - y-direction (from 0 to $-\Delta y$)
"a" denotes degrees of freedom on face a (i.e., at y = 0)
"b" denotes degrees of freedom on face b (i.e., at y = $+\Delta y$)
"c" denotes degrees of freedom on face c (i.e., at y = $-\Delta y$)

Using the Fourier expansion described earlier, forces and displacements are expressed as:

$$\hat{P}(m) = \int_{-\infty}^{\infty} \bar{P}(y)\, e^{imy}\, dy \tag{3.13}$$

$$\hat{U}(m) = \int_{-\infty}^{\infty} \bar{U}(y)\, e^{imy}\, dy \tag{3.14}$$

where $\hat{P}$ and $\hat{U}$ are used to represent vectors of nodal forces and displacements, respectively, in m space. Rewriting Equation 3.12 to incorporate the Fourier expansion of loads:

$$\begin{bmatrix} \bar{s}_{11}^{+} & \bar{s}_{12}^{+} & 0 \\ \bar{s}_{21}^{+} & \bar{s}_{22}^{+}+\bar{s}_{11}^{-} & \bar{s}_{12}^{-} \\ 0 & \bar{s}_{21}^{-} & \bar{s}_{22}^{-} \end{bmatrix} \begin{Bmatrix} \hat{U}_b(m) \\ \hat{U}_a(m) \\ \hat{U}_c(m) \end{Bmatrix} = \begin{Bmatrix} \hat{P}_b(m) \\ \hat{P}_a(m) \\ \hat{P}_c(m) \end{Bmatrix} \tag{3.15}$$

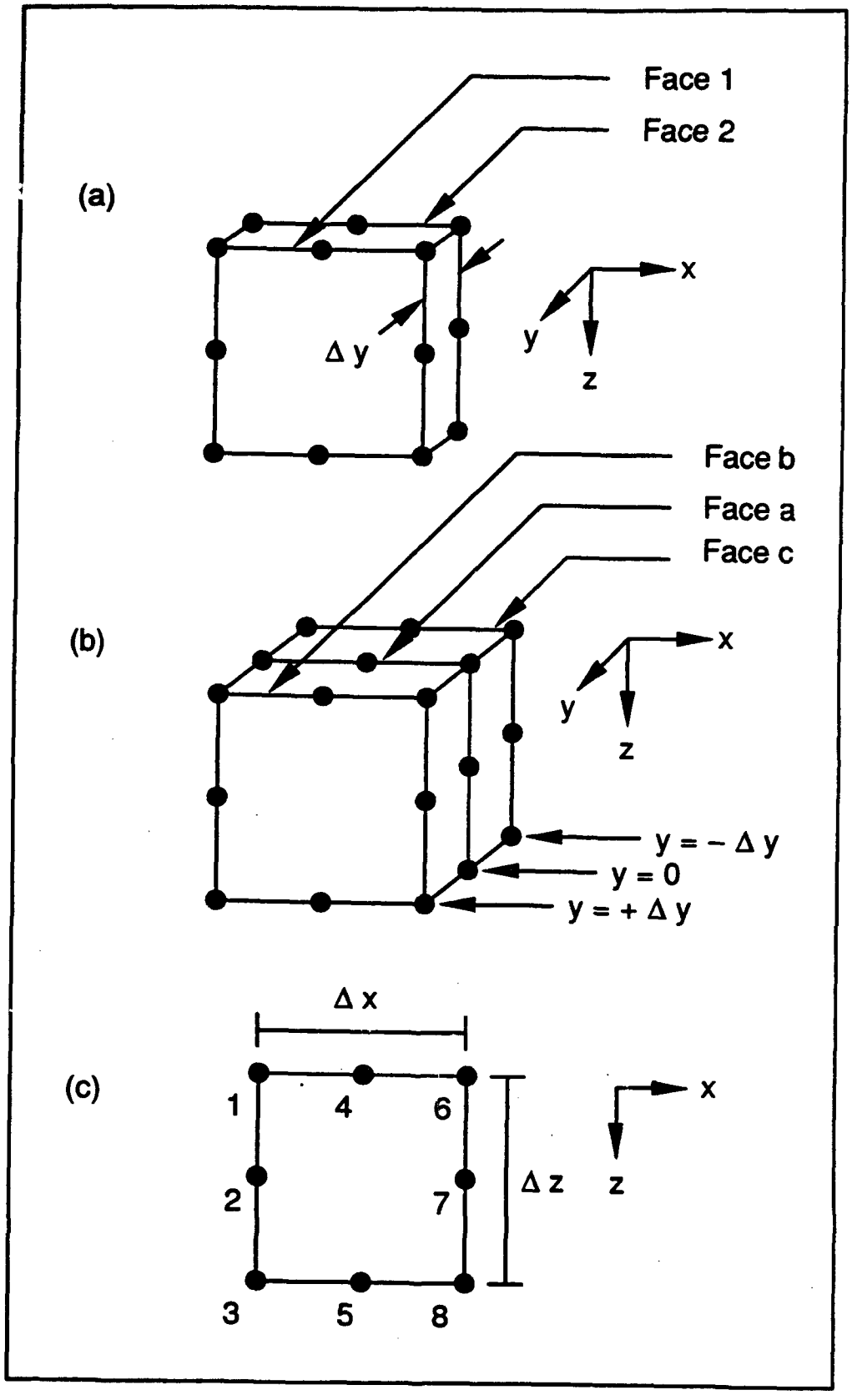

Figure 8. Condensation of finite elements adjacent in out-of-plane (y) direction

In the transform (m) space, the displacements on the "b" and "c" faces are related to the displacements on the "a" face at any instant in time by the simple relationships:

$$\hat{U}_b\ (m) = \bar{U}_a(m)\ e^{-im\Delta y} \tag{3.16}$$

$$\hat{U}_c\ (m) = \bar{U}_a(m)\ e^{+im\Delta y} \tag{3.17}$$

Defining:

$$\hat{s}(m) = \bar{s}_{21}\ e^{-im\Delta y} + (\ \bar{s}_{11} + \bar{s}_{22}\ ) + \bar{s}_{12}\ e^{im\Delta y} \tag{3.18}$$

which is not symmetric—the stiffness terms corresponding to displacements in the y-direction are out of phase. The stiffness matrix is made symmetric by multiplying the rows and dividing the columns corresponding to y-displacements by i and solving in terms of iv where v is the y-displacement. Equations 3.16 and 3.17 can be substituted into Equation 3.15 to get the system of equations for the equivalent two-dimensional system shown in Figure 8c:

$$\hat{s}(m)\ \hat{U}_a(m) = \hat{P}_a(m) \tag{3.19}$$

This formulation, then, allows the three-dimensional element with a two-dimensional geometry to be represented with an equivalent 2-D element.

Validation and Parametric Analysis

Validation studies were conducted to prove that the formulation and computer implementation are sound for the limited class of problems considered. The general accuracy of calculated displacements in terms of amplitude and phase was evaluated. A brief presentation of the results of the validation and parametric analysis are described below.

The best form of validation consists of comparisons with exact mathematical relationships for a suite of problems representing a wide spectrum of possible in-situ conditions. Comparisons with measured data from full-scale or prototype testing provide a constructive means to confirm findings when conducted under certain controlled conditions. Comparisons with measured data are not appropriate as the primary and only means of validation, however. Comparisons with other numerical approximations are even less appropriate for validation. Validation of *vib3* through comparisons with analytical results is possible only for the simplest class of planar geometry—a horizontally layered system extending to infinity. Green's function solutions formulated for axi-symmetric problems (with disk loads) by Kausel (1981)

were used exclusively with point and square loads (in plan). The same total area and a total load of unity were used to adequately equate problems with different load configurations.

The dynamic vertical displacements along the surface and sufficiently away from the load are of primary interest. Vertical vibrations are normally measured in non-destructive testing techniques such as the SASW method. Sensors are easy to align in the vertical position regardless of the surface slope. Measurements are likely to be made both perpendicular and parallel to the structure of the system (x- and y-directions, respectively). Therefore, the results are presented in terms of the variations of real and imaginary components of dynamic displacement in both horizontal directions—the x-direction (calculated at nodes on the $y = 0$ plane) and the y-direction (calculated at the node nearest the centroid of the load and expanded out in the y-direction). The variation of phase with distance is added to provide a means for closer examination.

Comparisons between the numerical approximations and closed-form solutions at distances from the source between 0.5 λ and 5.0 λ are excellent for nearly all of the cases considered. Examples of the close comparison are shown in Figures 9 through 11. The vertical components of dynamic displacement at the surface and at a depth of 0.8 λ are shown in Figures 9 and 10; respectively. Although not considered further in this report, the horizontal components of displacement at the surface are shown in Figure 11. The data in these figures as well as many other comparisons not shown confirm that the formulation and computer implementation are accurate.

Parametric analyses were conducted to assess the sensitivity of the formulation and numerical solution to system variables and to recommend thresholds for these variables. The formulation was found to be sensitive to the following system parameters: the spatial increments of discretization in all three directions and the total length of discretized space in the y-direction. The results are also moderately sensitive to reasonable ranges of Poisson's ratio and damping for soils. The solution accuracies are not sensitive to the width of the load using reasonable bounds of load width, soil velocities, and operating frequencies. The calculated displacements were shown to be slightly more accurate as damping ratio was increased from 2 to 5 percent.

Comparisons were also made between the time and memory requirements to execute *vib3* and an equivalent solution model using a commercial 3-D FEM software package (*ABAQUS*). The semi-analytical method was found to generally be 25 times faster and use only one-fourth the CPU memory space. Therefore, the new code is an accurate and economical alternative to expensive 3-D modeling.

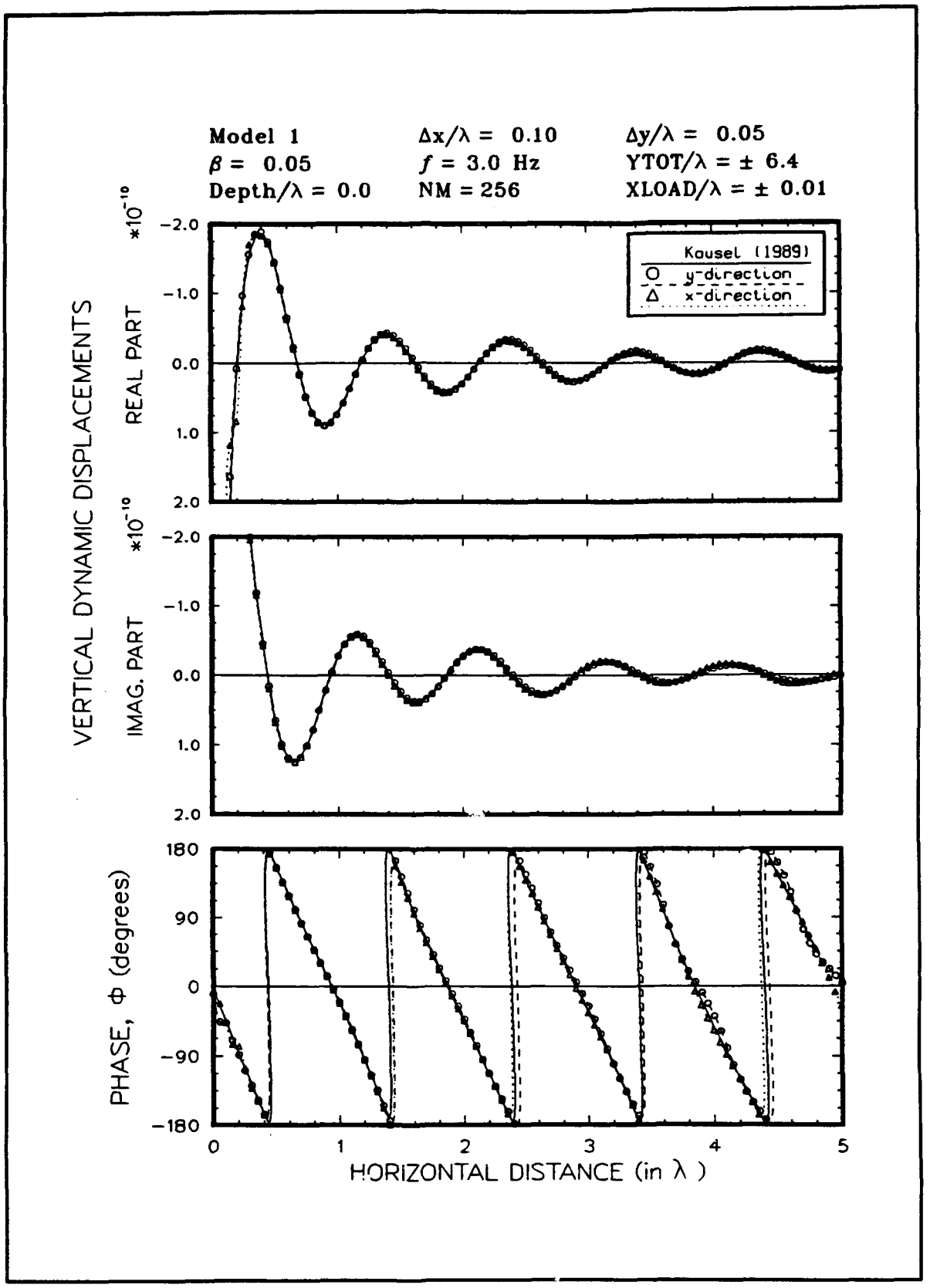

Figure 9. Comparison between calculated vertical displacements and Green's function solution along surface

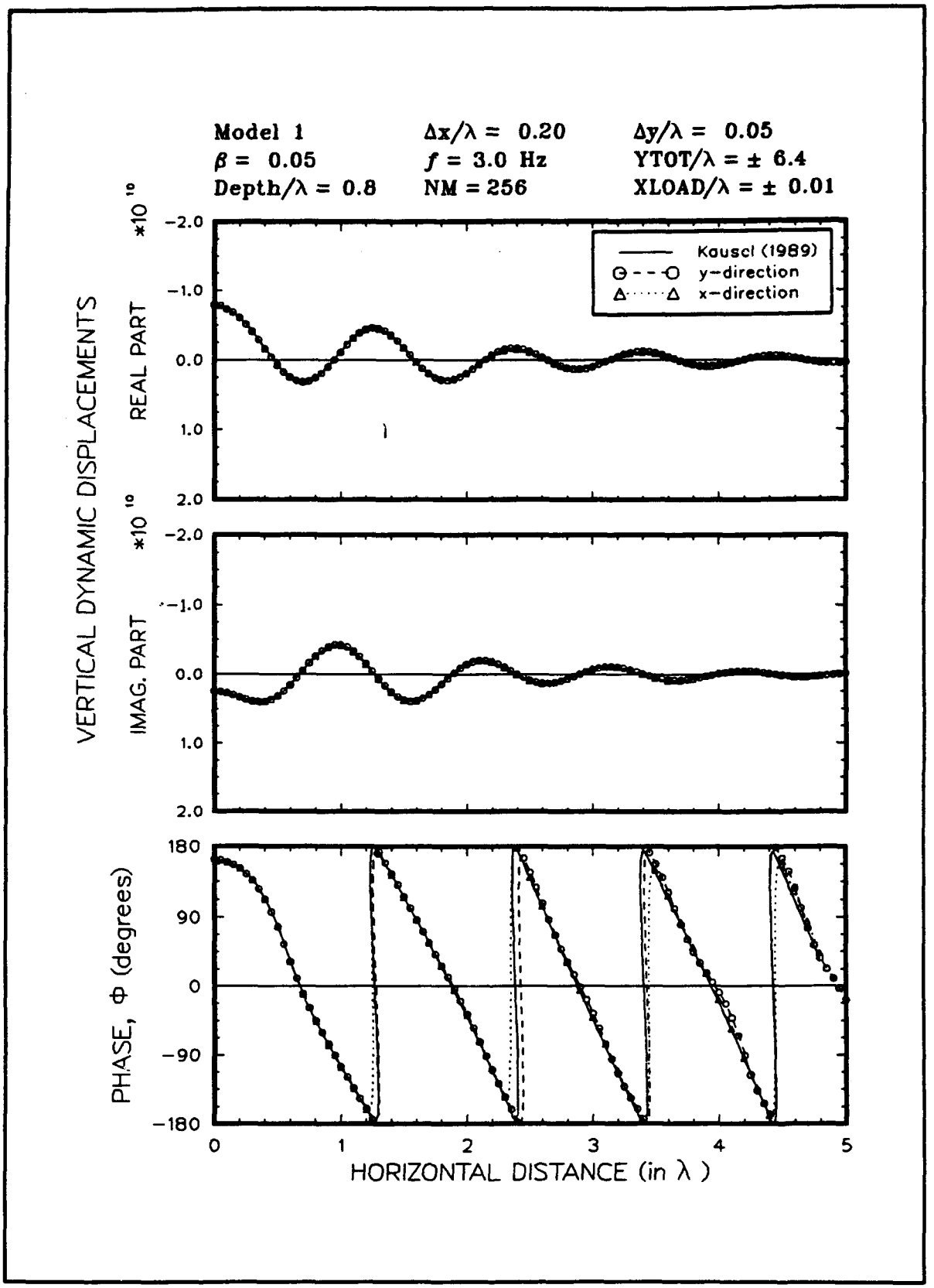

Figure 10. Comparison between calculated vertical displacements and Green's function solution at depth of 0.8 λ

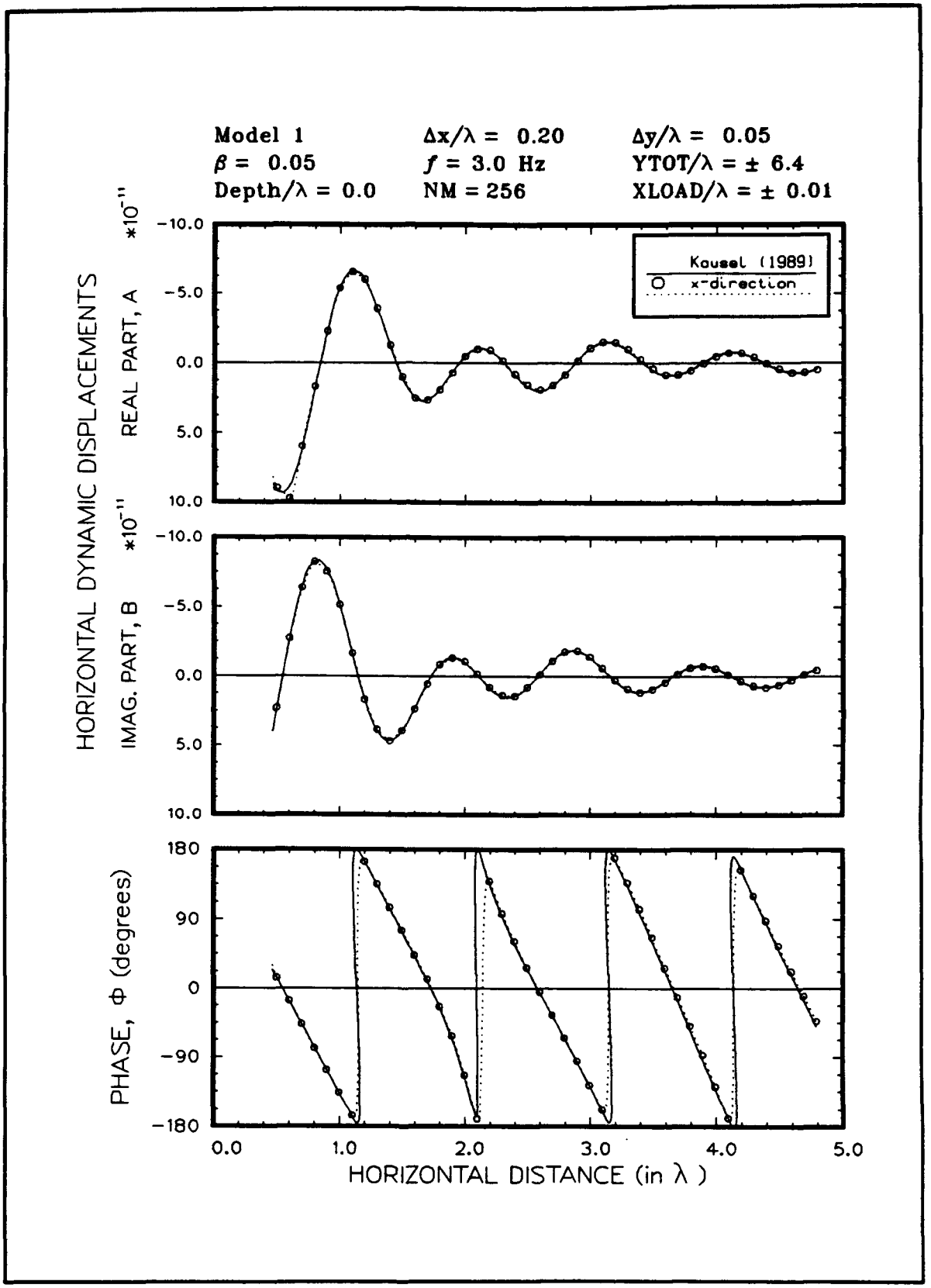

Figure 11. Comparison between calculated horizontal displacements and Green's function solution along surface

4 Results of Computations

This chapter is used to describe the results of analyses compiled with the semi-analytical method. The variations of dynamic vertical displacements in the x-direction (direction of maximum topographic gradient) and the y-direction (direction of zero topographic gradient) were calculated and analyzed to define trends that can be used with inversion schemes to derive material stiffness. The slope was assumed to extend to infinity.

Several researchers have examined the effect of surface discontinuities on the amounts of surface wave energy transmitted and reflected using laboratory measurements. The collection of their results is somewhat inconsistent but does show a strong dependence on the slope angle. A few have also examined the effect of surface discontinuities on phase. These results indicate that the effect of slope angle can be easily avoided or taken into account.

The variables defining the problem are shown in Figure 12 with the slope angle, α, and the load set-back distance, x_{LC}, being the primary variables; infinite slope conditions were modeled. Square loads were used throughout and can be related to circular load areas by use of equivalent total loads. Calculations were made using six common engineering slope ratios (horizontal:vertical)—1:1, 1.5:1, 2:1, 2.5:1, 3:1, and 6:1. The load was placed at the top and base of the slope with these ratios to produce α = 135, 146, 153, 158, 162, 171, 189, 198, 202, 207, 214, and 225 degrees. (An α of 180 degrees corresponds to the level ground conditions considered in previous chapters.) The center of the load was used as the reference point for distance measurements. Unit-less dimensions are used for convenience. The shear wave velocity was fixed at 1000 with 5 percent damping. The mass density and Poisson's ratio were 4.00 and 0.40, respectively, producing a V_R equal to 940.

The results of computations were initially evaluated to determine the effect of system parameters. Thresholds defined by Sykora (1993) for level ground conditions were generally found to be appropriate for sloping ground conditions. Free and fixed (rigid) boundaries of the discretized FEM models were placed at sufficient distances to avoid any effects in the regions of comparison.

One initial finding was that the phase velocities calculated from measurements along an infinite, homogeneous slope are independent of the harmonic

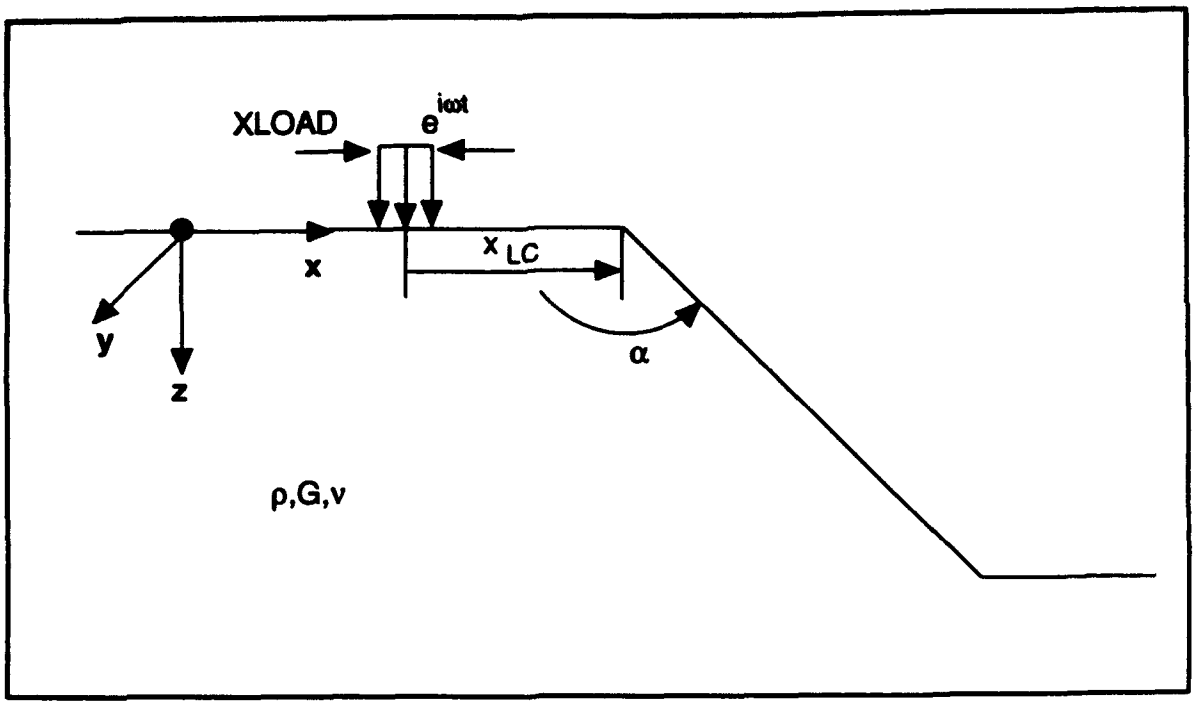

Figure 12. Schematic of problem variables used to analyze surface wave propagation in sloping ground

frequency of excitation (i.e., non-dispersive). This finding is consistent with level ground conditions and greatly simplifies the analysis of data for sloping ground conditions.

The variations of vertical displacement and phase at a slope, ϕ_s, for a slope ratio of 1.5:1 (α = 146 degrees when the load is at the crest of the slope and α = 214 degrees when the load is at the base of the slope) are shown in Figures 13 and 14, respectively. The relative location of the discontinuity along the abscissa is shown as a vertical dashed line. The level-ground solution (Kausel 1989) is also shown for comparison.

The primary effect of the slope discontinuity is a phase shift for waves traveling in the direction of maximum topographic gradient that occurs between the discontinuity and a distance of $3\lambda/4$ beyond (when $x_{LC} = 1.0\ \lambda$). The phase difference becomes essentially constant at greater distances. The phase has a marked lag from the level ground solution at distances beyond the discontinuity when α = 146 degrees and a marked phase lead when α = 214 degrees. The calculated solutions in the y-direction along the crest and base correspond well to the level-ground solution, regardless of α.

The amount of phase shift at these two slope angles was examined by comparing the total (unwrapped) phase with the total phase from level ground (Green's function) solutions, ϕ_g, and the total phase produced by a uniform increase of 360 degrees per wavelength and passing through the origin, ϕ_{360}. These differences are shown in Figures 15 and 16, respectively. The ϕ_{360} is used to calculate dispersion curves for the SASW method and a comparison

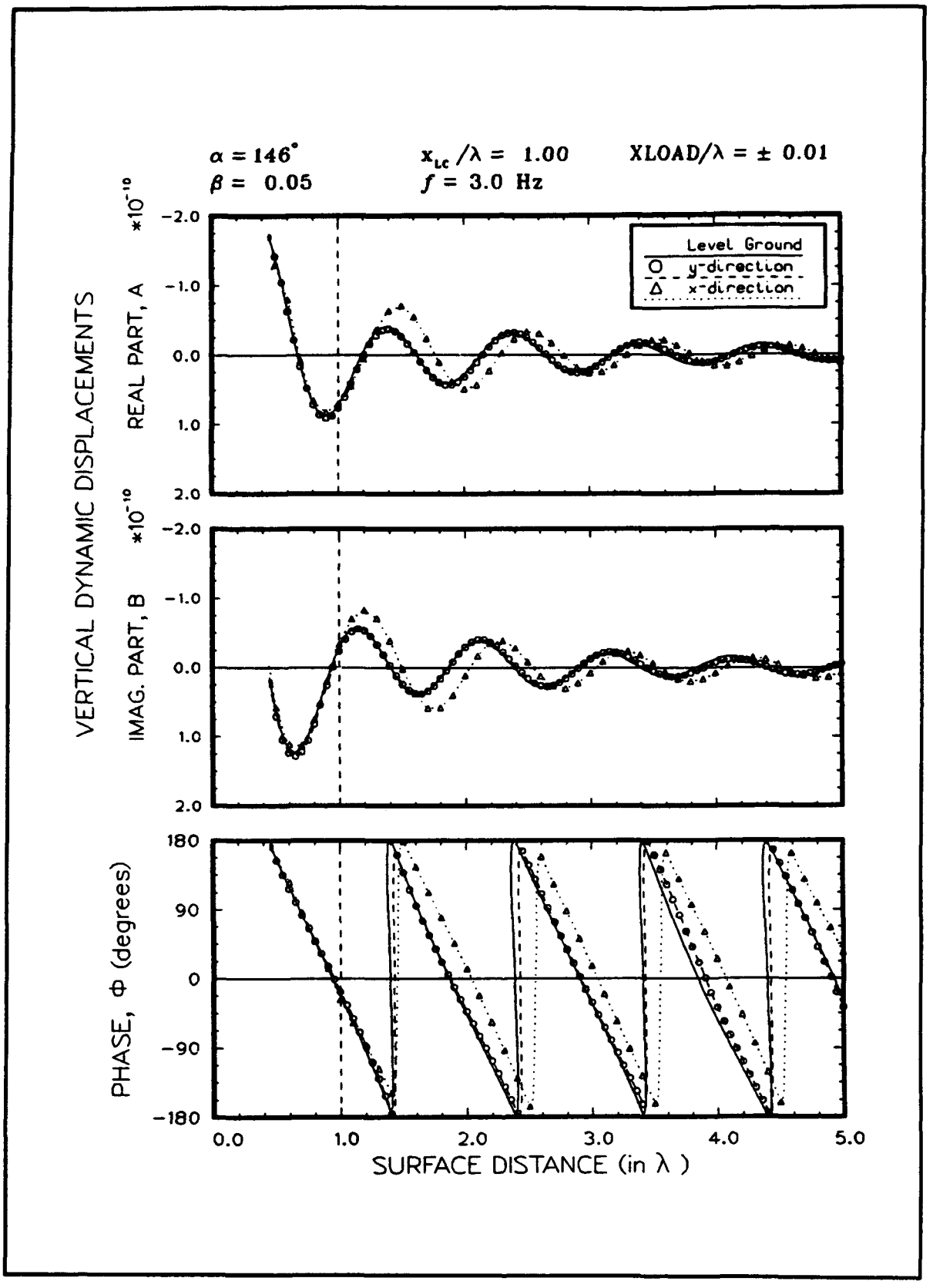

Figure 13. Variation of displacements and phase for α = 146 degrees

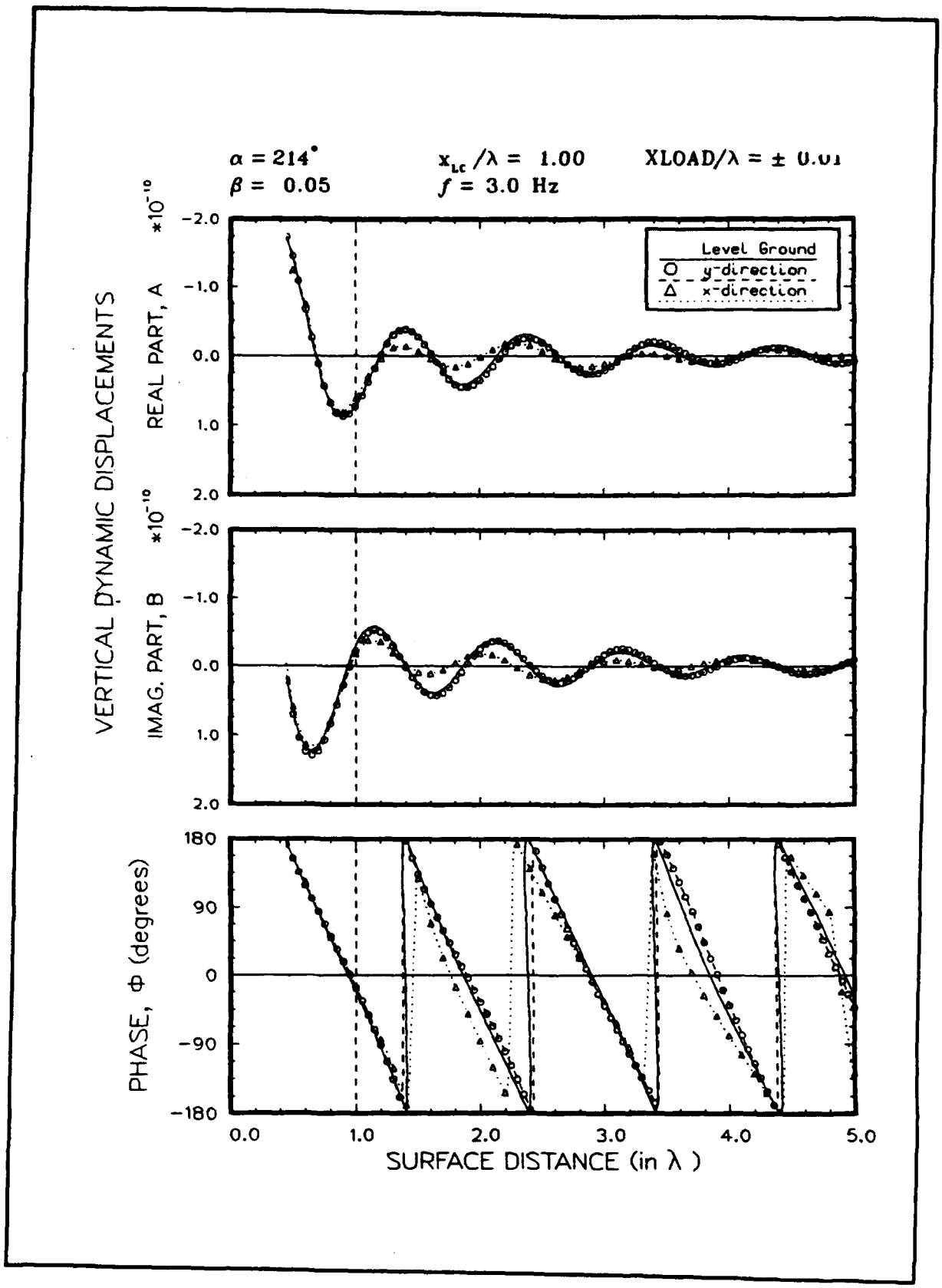

Figure 14. Variation of displacements and phase for α = 214 degrees

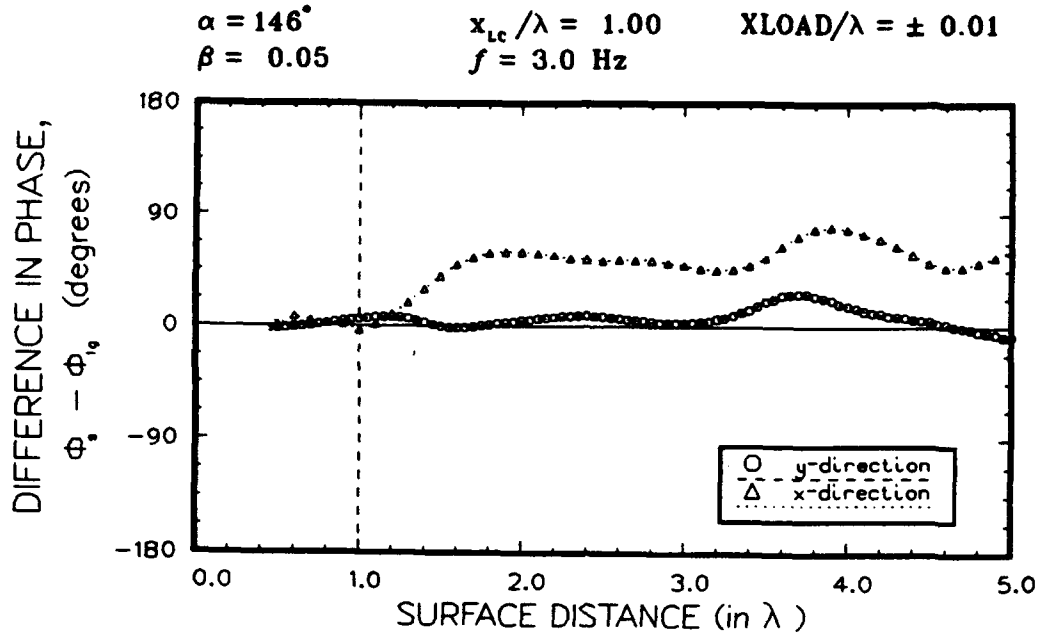

a. α = 146 degrees

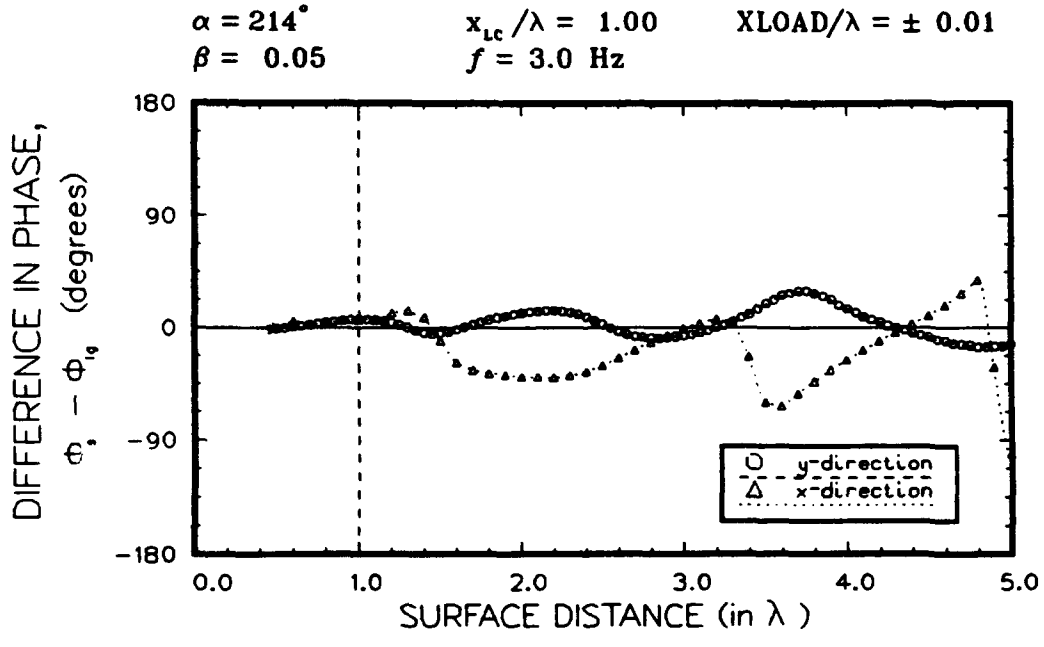

b. α = 214 degrees

Figure 15. Difference in phase between sloping ground and level ground conditions

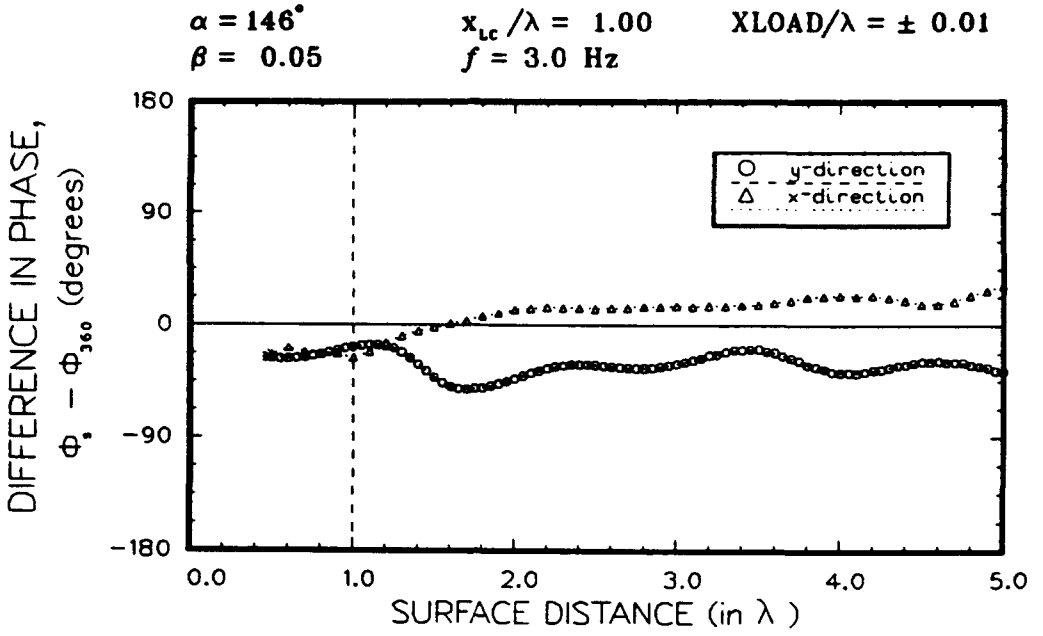

a. α = 146 degrees

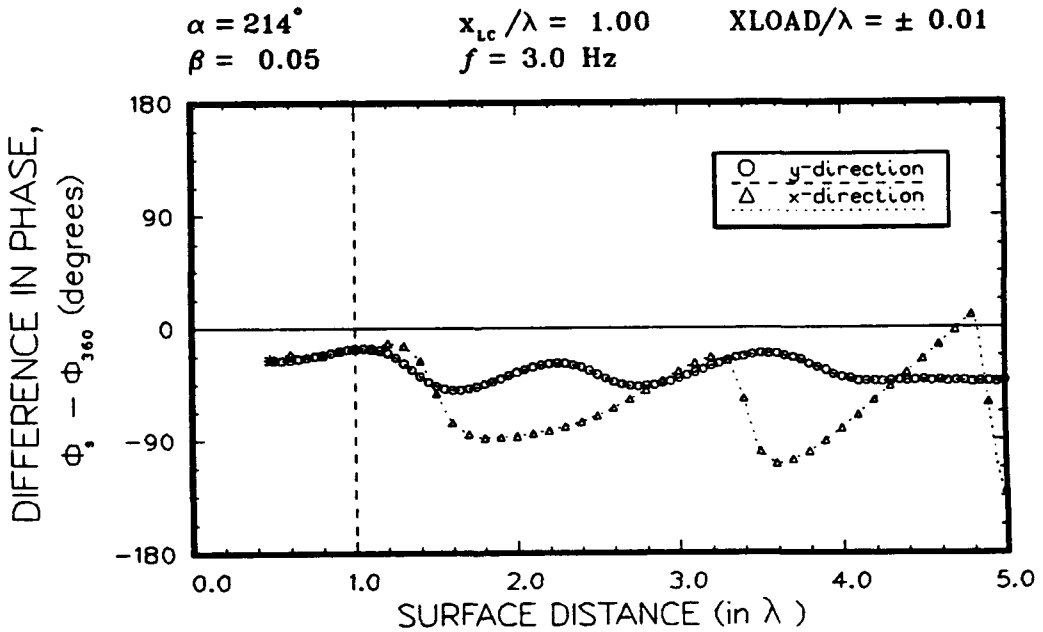

b. α = 214 degrees

Figure 16. Difference in phase between sloping ground and a uniform increase of 360 degrees per wavelength

between ϕ_{lg} and ϕ_{360} is shown in Figure 17. The phase difference between the two vertical values approaches 60 degrees at distances less than 5λ when $\nu = 0.40$.

The difference in phase between sloping and level ground conditions in Figure 15 shows the relatively-small magnitude of phase shift. The variation of phase difference after the shift, beyond distances of about 3λ/4 from the discontinuity, is relatively constant when $\alpha = 146$ degrees. The small fluctuations that exist are similar to those for the solution along the crest. The overall variation of phase in the x-direction when $\alpha = 214$ degrees is much larger and less consistent. Along the base and crest there is no noticeable phase difference and the magnitude of fluctuations is small.

The difference in phase between sloping conditions and ϕ_{360} is shown in Figure 16. Both sets of data have shifted down relative to the data shown in Figure 15 because of the difference between ϕ_{lg} and ϕ_{360} noted previously. The differences along the crest and down the slope for $\alpha = 146$ degrees again are both relatively constant. These data strongly suggest that measurements can be reliably used in both the x-direction (down the slope) and the y-direction to determine soil stiffness using the SASW method, especially if the receivers are placed at a distance greater than 3λ/4 beyond the discontinuity to avoid the phase shift.

The results when $\alpha = 214$ degrees are not as consistent. The phase difference appears to vary considerably at surface distances beyond the initial phase shift. The general trend at distances greater than 2.5 λ is for the phase to decrease uniformly (lag) as a ratio of distance until a sudden shift occurs (e.g., at 3.4 λ). This type of response is not desirable for methods such as the SASW.

The variation of phase from a larger perspective indicates that the differences shown in Figures 15 and 16 may not be of importance from a practical standpoint. The variation of unwrapped phase with distance for most slope angles (minor discontinuities not included) are shown in Figures 18 and 19. Also shown in Figure 18 are lines corresponding to a least squares linear fit of data between surface distances of 1.0 and 5.0 λ for each slope angle.

The data in Figure 18 shows that the distribution of unwrapped phase is fairly consistent and unique when $\alpha < 180$ degrees. The best-fit segments at these angles effectively represent a variation of phase between 360 and 350 degrees per wavelength. The increased variation in phase when $\alpha > 180$ degrees is also seen in Figure 18 although the best-fit linear segments are very similar and are close to ϕ_{360}. The error associated with this variation is small and can be minimized by using large spacings. The data in Figure 19 clearly shows the independence of phase change along the crest and base to α and how close the phase is to ϕ_{360} (shown as a line segment in Figure 19).

The phase shifts for all α considered using the differences shown in Figure 16 were plotted in Figure 20. The difference in phase is not zero at

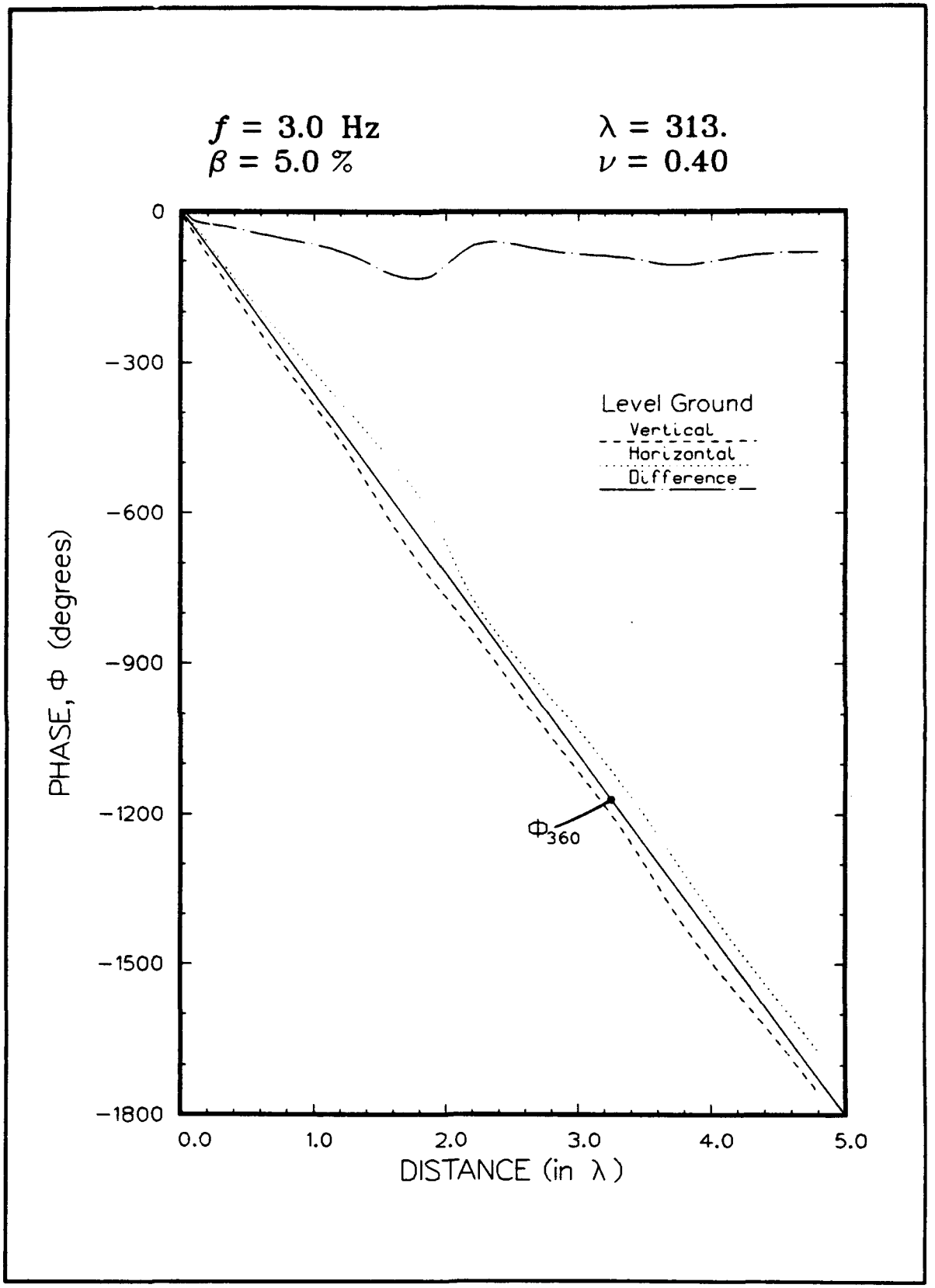

Figure 17. Difference in Green's function solutions for horizontal and vertical components (Kausel 1989)

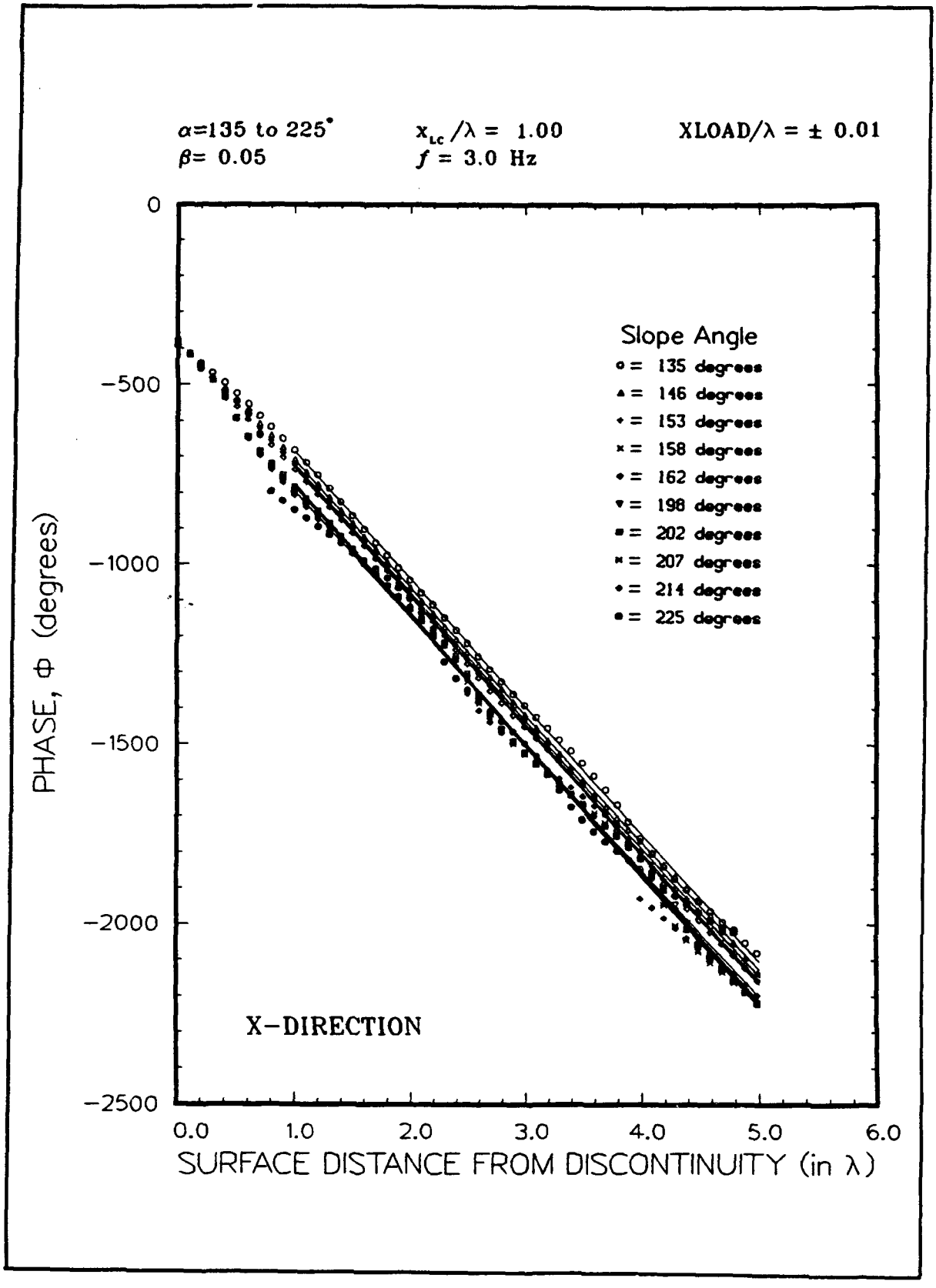

Figure 18. Variation of phase in direction of greatest topographic gradient

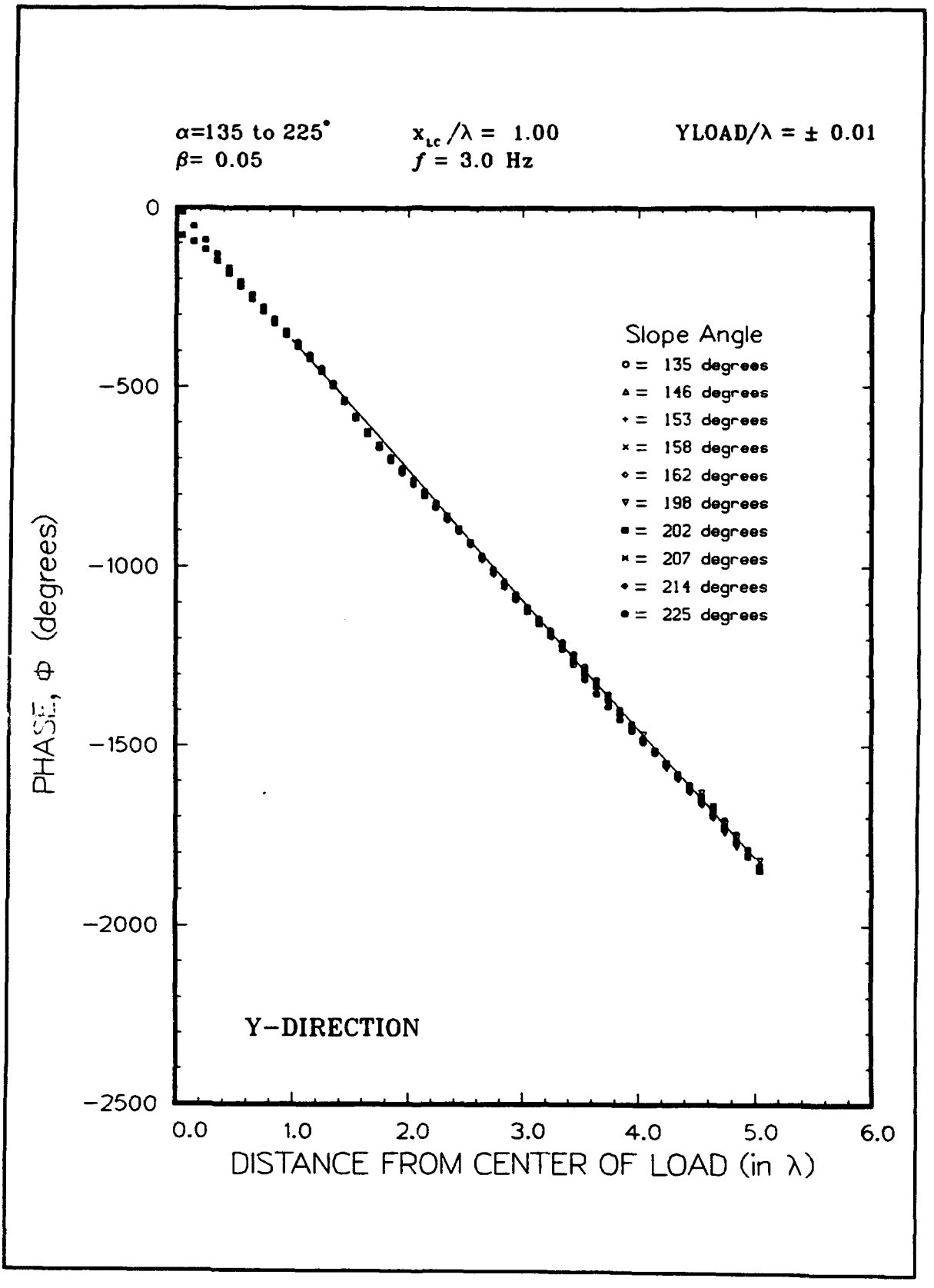

Figure 19. Variation in phase in direction of zero topographic gradient

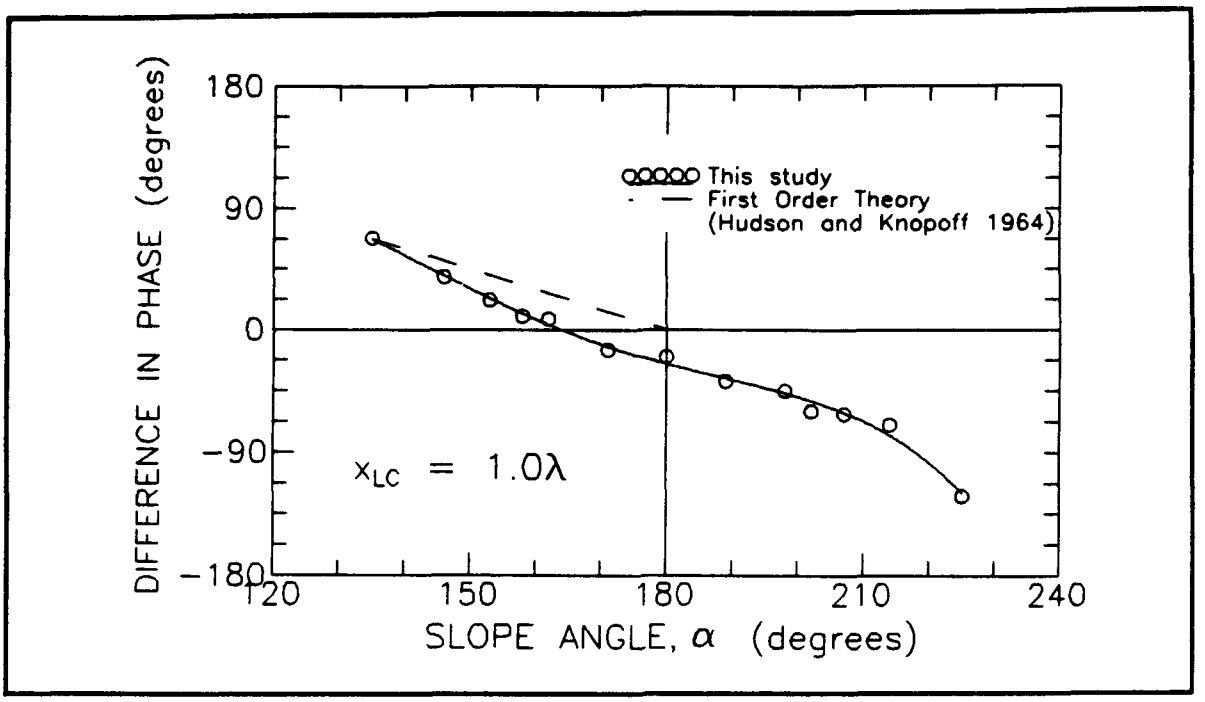

Figure 20. Variation of phase shift with slope discontinuity angle

α = 180 degrees which reflects the difference between ϕ_{ls} and ϕ_{360}. These results are smaller than "first-order theory" (no surface wave reflections included) reported by Hudson and Knopoff (1964). Although it appears possible to predict the phase shift caused by a surface discontinuity, calculated phase velocities are likely to be more accurate if this phase shift is avoided in the analysis. The difference in phase as a function of α was found to be independent of x_{LC} as long as $x_{LC} > 0.5\ \lambda$.

The real and imaginary parts of peak displacements at distances beyond the discontinuity amplify as α decreases from 180 degrees and deamplify as α increases above 180 degrees. The ratio of peak vertical displacements as a function of α to peak vertical displacements for level ground are shown in Figure 21. This ratio is a function of x_{LC} and tends to be a maximum when x_{LC} is about 1.0 λ. A standard set-back distance of 1.0 λ was used for most analyses.

The combined results suggest that measurements made along the crest or base of a slope can safely be processed using existing SASW inversion schemes to obtain stiffness profiles. Phase velocities representing measurements down a slope can also be reliably obtained from vertical measurements. The best method would be to place receivers beyond $3\lambda/4$ thus avoiding any interpretation. Much more variation is expected for measurements made up a slope. For homogeneous systems, the phase velocity will closely approximate V_R.

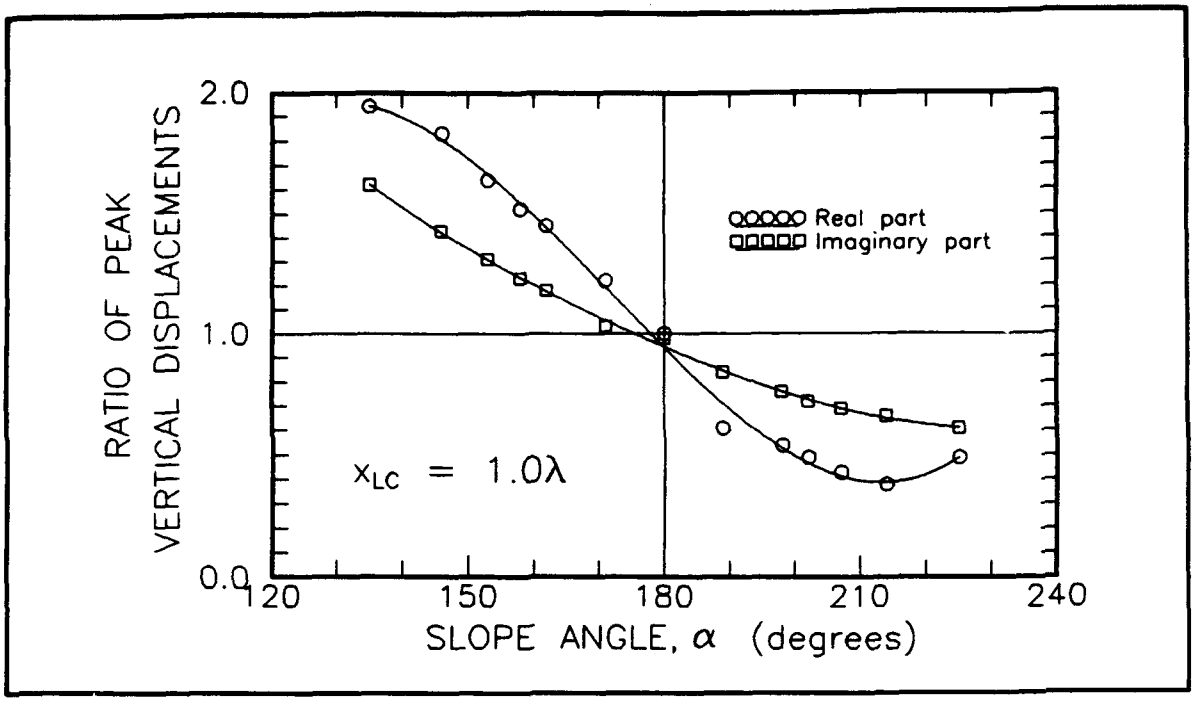

Figure 21. Variation of ratio of peak vertical displacements with slope discontinuity angle

5 Field Measurements

Field measurements of vertical dynamic displacements on level ground and sloping ground were made on the WES Reservation in Vicksburg, Mississippi, during the month of August, 1993. These data allow comparisons between the results of numerical analyses and physical measurements, particularly since exact solutions do not exist for sloping ground. A secondary purpose for conducting the field program was to evaluate the effect of seismic sources and sensor spacings on measured displacements. Discussions about the response produced by different combinations of these two factors are included below.

The site is located about 100 yards northeast of the Casagrande Building and adjacent to Porter's Chapel Road. It consists of a road cut with a maximum height of 25 ft and slope angles (using the convention presented in Figure 12) between about 155 and 165 degrees and a concrete bridge with a steel support system. A site map is provided in Figure 22 and a photograph of the bridge is shown in Figure 23. The southern portion of the site is flat and level but a short road embankment which serves as an approach for the bridge exists on the eastern margin. The crest of the cut slope lies in an ESE-WNW direction.

Natural soil consists of Pleistocene-age loess indigenous to the Vicksburg area. This loess is uniformly graded and typically has a low unit weight. Groundwater does not exist within the depths tested. During testing, the ground surface was very resistant to penetration which is attributed to desiccation.

Some shallow fill may also exist across the site, the consequence of site grading during construction. An embankment fill was used beneath the county road as an approach to the bridge.

General Procedure

A field testing program was designed to determine the stiffness profile on level ground (free field) to a depth of about 25 ft and to measure dynamic vertical displacements along the crest and down the slope at two locations. The general locations of the arrays are shown in Figure 22. Both impulsive and harmonic wave sources were used. Impulsive sources were hammer

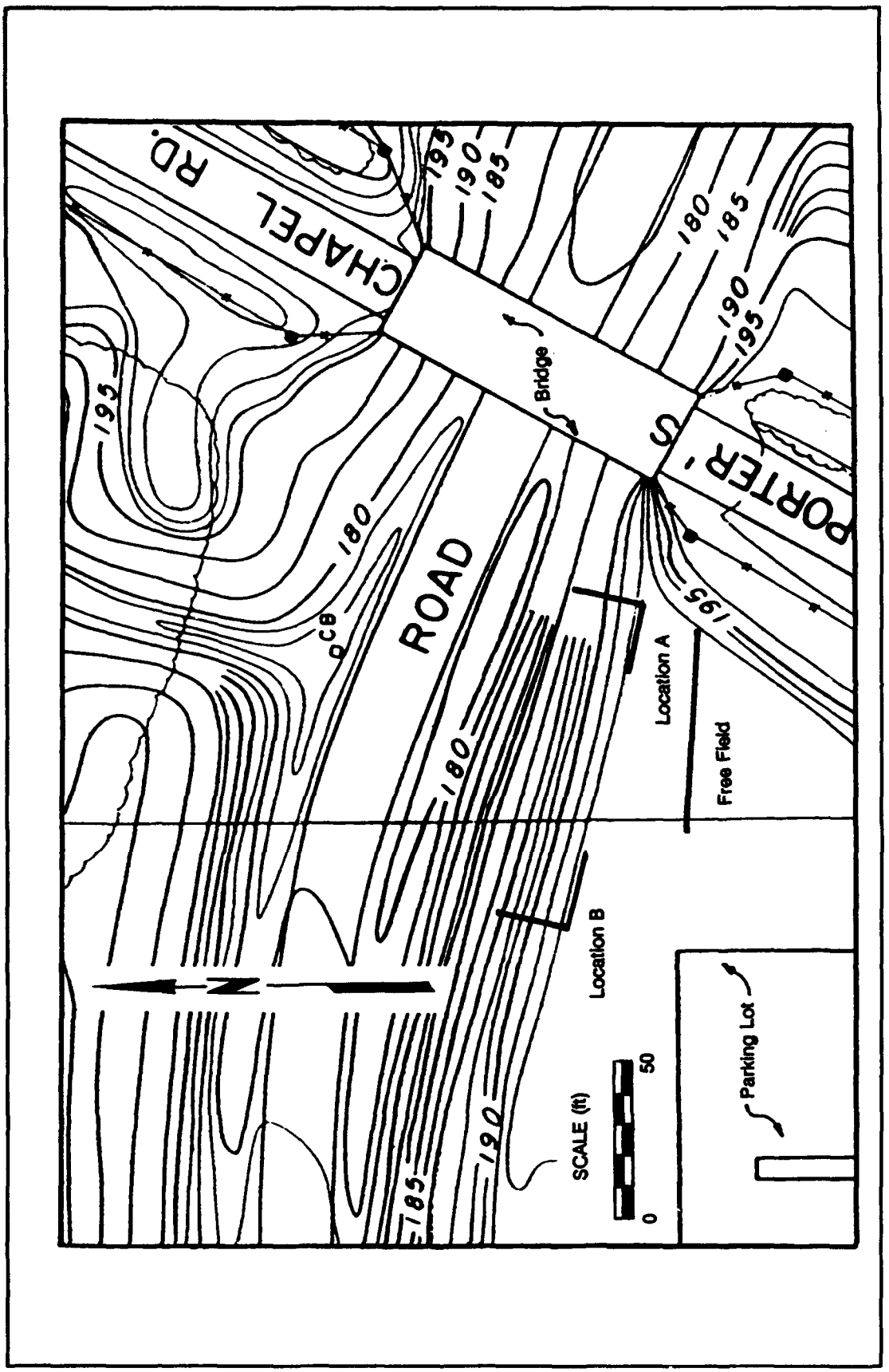

Figure 22. Site map of WES test site

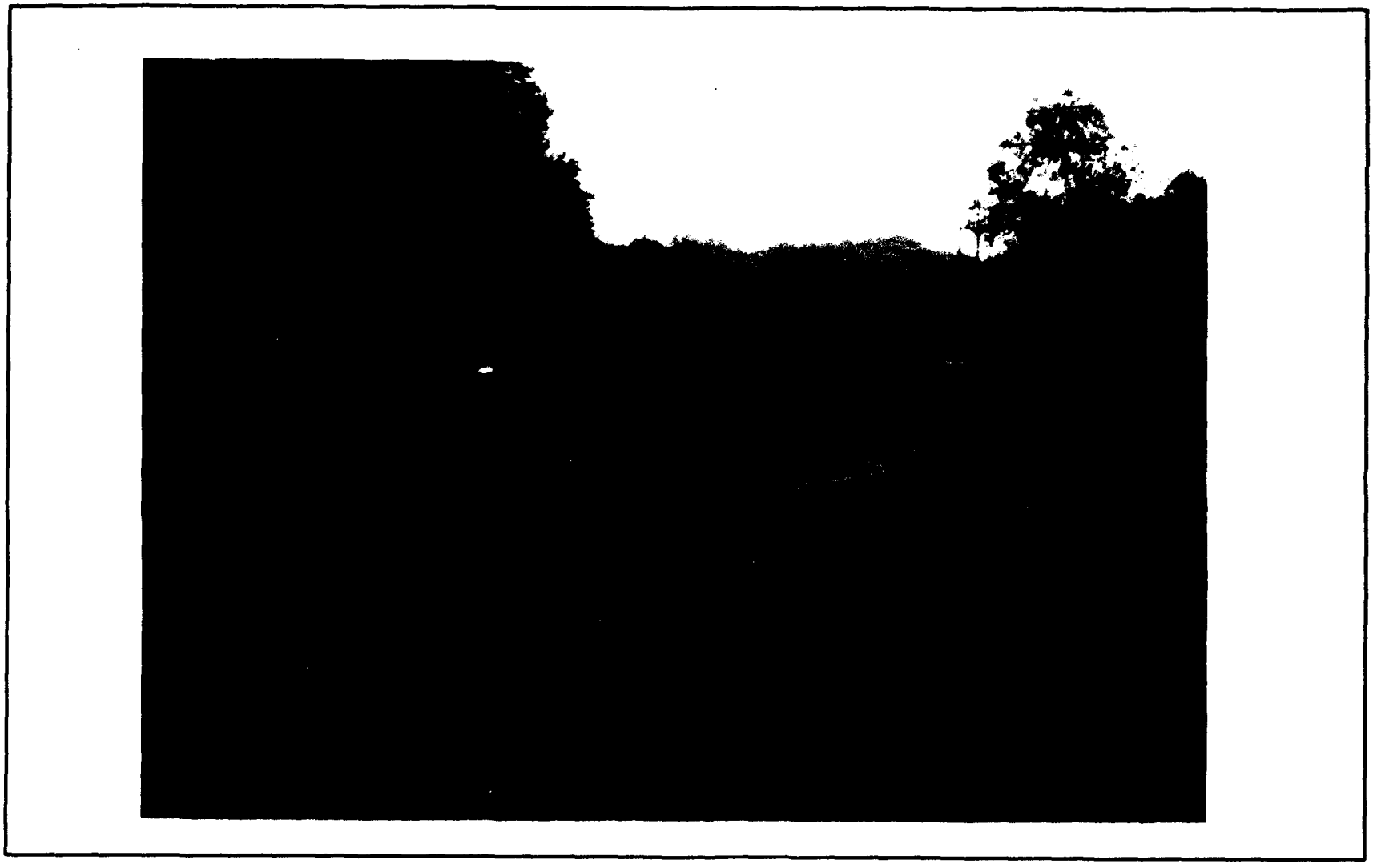

Figure 23. View of bridge at WES test site looking east with area of seismic measurements on sloping ground in foreground

blows, dropping of a boulder, and activation of a Dynatest Falling Weight Deflectometer (FWD). Greater energy is typically required as the spacing increases as was the case at this site. The harmonic excitation was produced using a 50-lb Goodman electro-magnetic vibrator with a platen diameter of 6 in. A Hewlett Packard 3562A dynamic signal analyzer was used to produce the input signal and to collect, analyze, and store signals. An overall view of the equipment used for measurements with harmonic loads is shown in Figure 24.

Averaging of signals was used for collecting data from both source types. For impulsive sources, five time-domain signals were averaged and stored digitally using the HP spectrum analyzer (example shown previously in Figure 2). For harmonic source measurements, the vibrator was programmed to run a swept-sine test between frequencies of 25 and 325 Hz at increments of 0.375 Hz. Five cross-correlations and coherency relationships between the source and each receiver were averaged at each frequency and stored (example shown previously in Figure 3).

Dispersion curves were developed from data respective of each location and direction. Inversion techniques developed by Nazarian (1984) and adapted by WES (Alexander 1992) were employed to develop dispersion curves for data collected with impulsive sources (refer to Chapter 2). The variation of phase and coherence calculated from a cross power spectrum between the two averaged signals with frequency are the primary relationships used for this process. Dispersion curves for data collected using the harmonic source were easily derived by subtracting values of (unwrapped) phase between the two receivers and using Equation 2.6.

Level Ground Measurements

The testing configuration for level ground measurements is shown in Figure 25 and follows the common-midpoint procedure with $d_2/d_1 = 2$ (except for Test F10 where $d_2/d_1 = 1.7$). Velocity transducers (Mark Products L-22) with a resonant frequency of 2 Hz were positioned in an attempt to avoid the effects of the nearby slope, pavements, and structures. Both impulsive and harmonic sources were used to measure surface wave displacements in level ground. However, the dispersion curve and stiffness profile were derived only from measurements using the impulsive source.

The presence of an embankment, even a short embankment, was found to introduce some scattering of the signal. Consequently, waves traveling east (Tests F1, F3, and F6) were not used to evaluate stiffness. The variation of phase and coherence with frequency calculated from hammer blows at a spacing of 8 ft in opposite directions (Tests F3 and F4) are shown in Figure 26. The data from Test F3 correspond to sensors being located between the source and the county road embankment; the data from Test F4 correspond to sensors being located in the direction away from the road and source. The sources were 60 ft and 36 ft from the base of the embankment for tests F3 and F4,

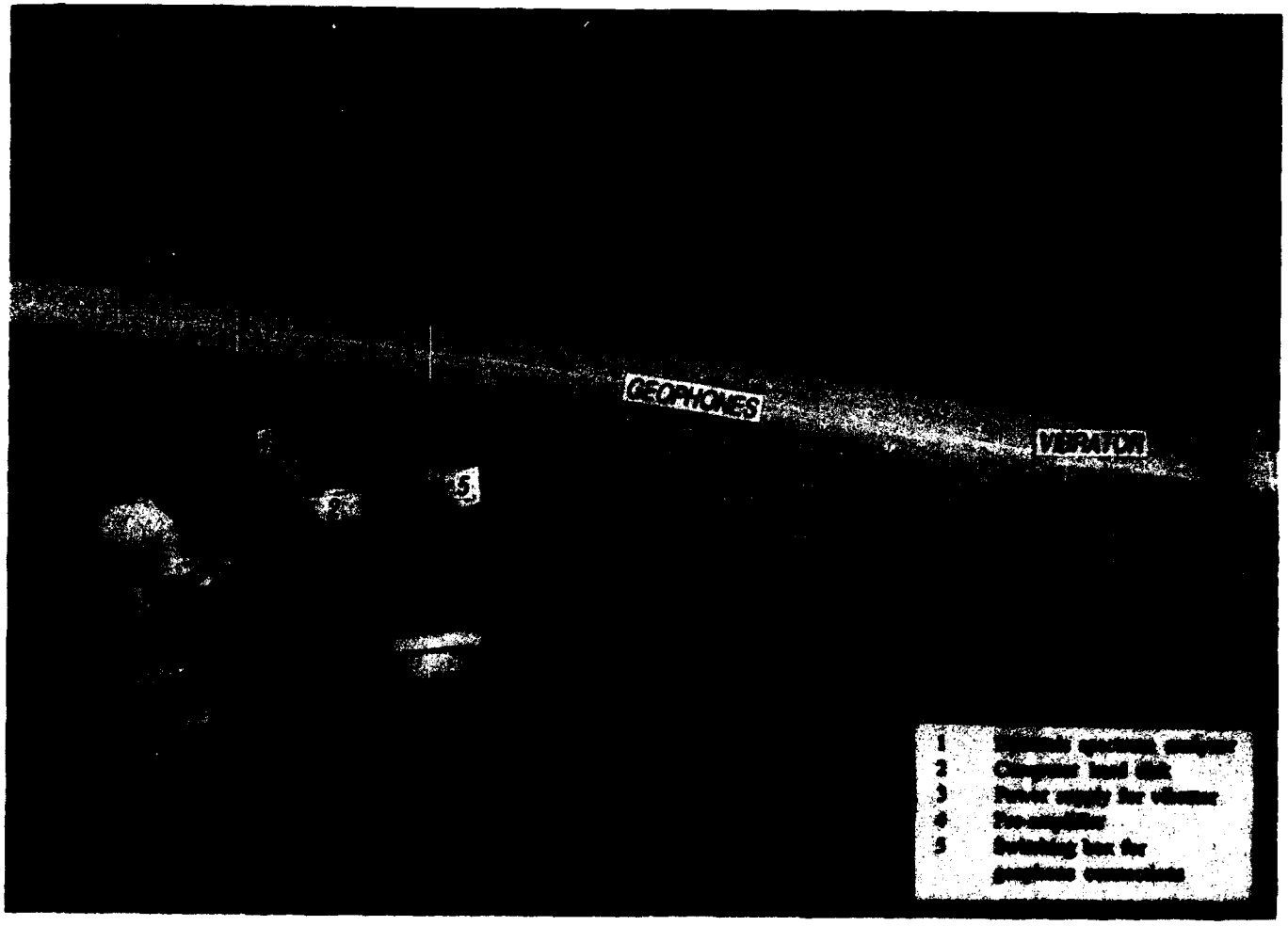

Figure 24. Equipment and layout used for measurements produced by harmonic loads

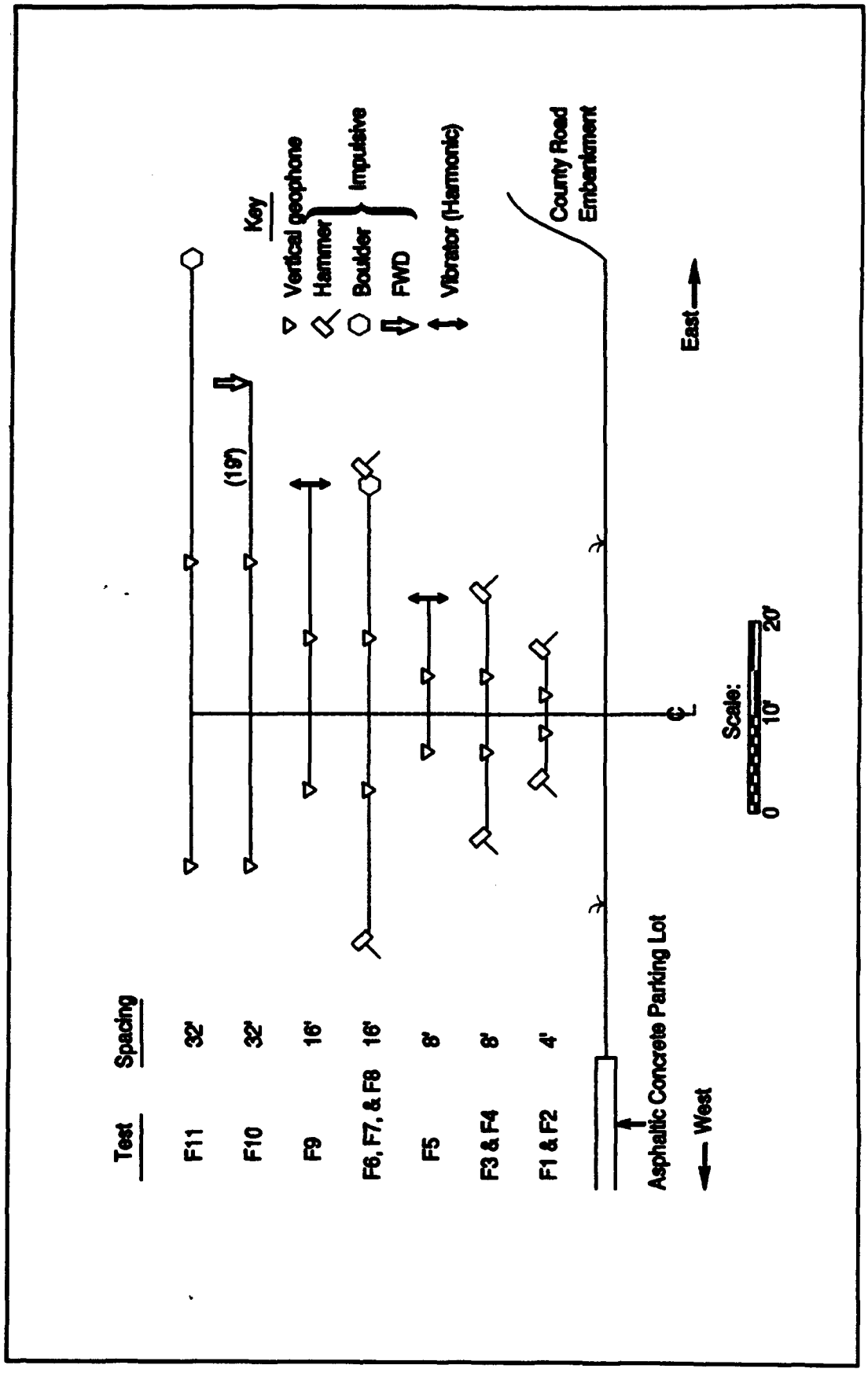

Figure 25. Testing configuration for level ground measurements

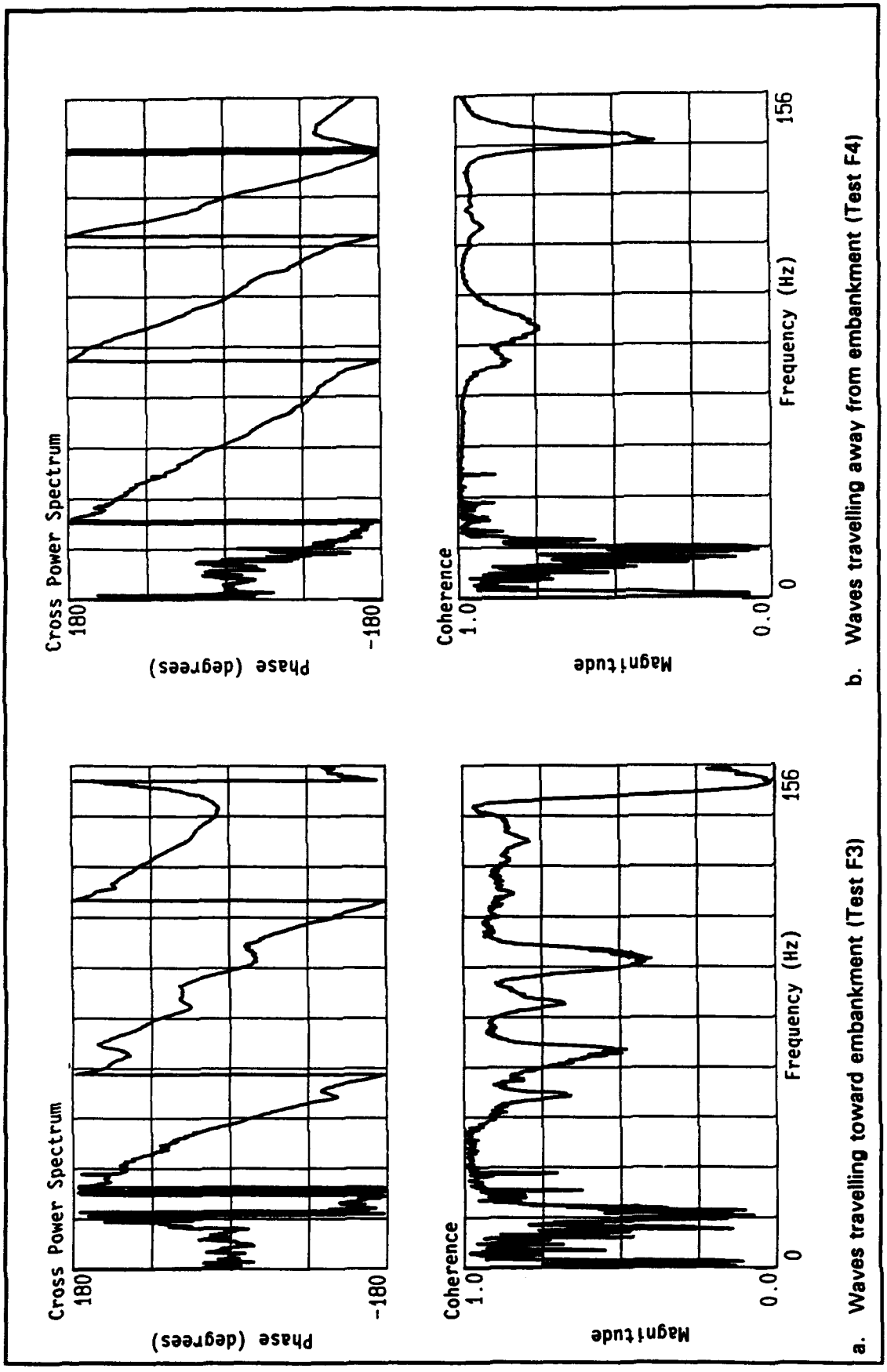

Figure 26. Phase difference and coherence between receivers at 8-ft spacing produced by averaged hammer blows in level ground

respectively. The phase relationship for waves traveling away from the embankment is much smoother and the coherence is generally higher for frequencies between 25 and 125 Hz. Similar findings were made at other spacings.

A significant difference was found to exist in the energy imparted by the boulder and the FWD for the level ground measurements. Corresponding signals for Tests F10 and F11 are shown in Figure 27. The coherence produced using the FWD at frequencies greater than 15 Hz are quite large, much better than the coherence produced using the boulder. A comparison of phase relationships is less conclusive, however. Based on this comparison, it would appear that the FWD is a good source for large spacings on level ground, much better than a boulder.

The level ground site was found to have a non-uniform profile of stiffness (which was the assumption for numerical calculations). The dispersion curve for level ground measurements using all three impulsive sources is shown in Figure 28 with the individual test data indicated. A best-fit relationship used for inversion is also shown. The phase velocity generally increases as a function of depth to the power of 0.27. A comparison between final iterated points along the dispersion curve and measured data is made in Figure 29. The stiffness profiles produced using the best-fit relationship of the dispersion curve assuming a Poisson's ratio of 0.40 and a density of 100 pcf is shown in Figure 30. The increments in modulus with depth produce a relatively uniform increase with depth (2,200 psf per ft depth) except between depths of 6 to 11 ft where the increase is slightly less.

Sloping Ground Measurements

The locations of the slope arrays were shown previously in Figure 22. The testing configuration for slope measurements and additional photographs of these areas are shown in Figures 31 through 33. The slope angles measured using a level survey at Locations A and B are 160.5 and 163 degrees, respectively. The testing configuration was selected to avoid measuring phase shifts near the discontinuity and allow the use of a wide range of frequencies. Twelve velocity transducers (Mark Products L20 DX's) with a resonant frequency of 14 Hz were positioned vertically at locations down the slope and along the crest (toward the other array location) at 1-ft spacings between distances of 10 and 21 ft from the center of the source platen. (At site A, only 10 geophones were used down the slope. In addition, the data at a surface distance of 16 ft were inadvertently not stored.)

In most instances, the phase and coherence for measurements using a harmonic source for sloping ground conditions are nearly ideal for processing. One such set of phase and coherence data is shown in Figure 34. The phase is nearly linear and the coherence is usually greater than 0.99 except at frequencies less than 50 Hz and greater than 250 Hz. Aliasing of phase relationships typically began to occur at wavelengths less than 3 ft (frequencies

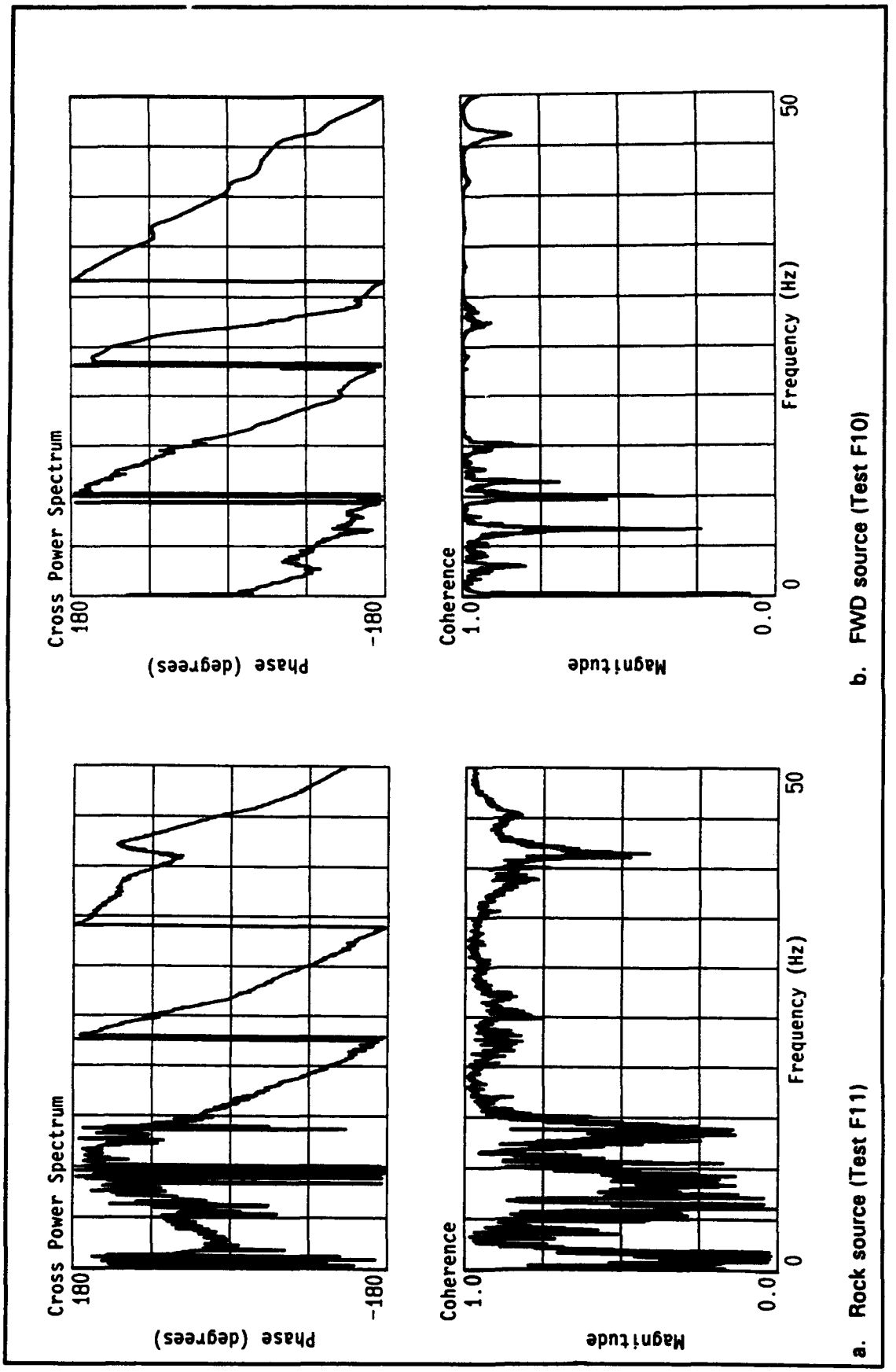

Figure 27. Phase difference and coherence between receivers produced by averaged blows in level ground

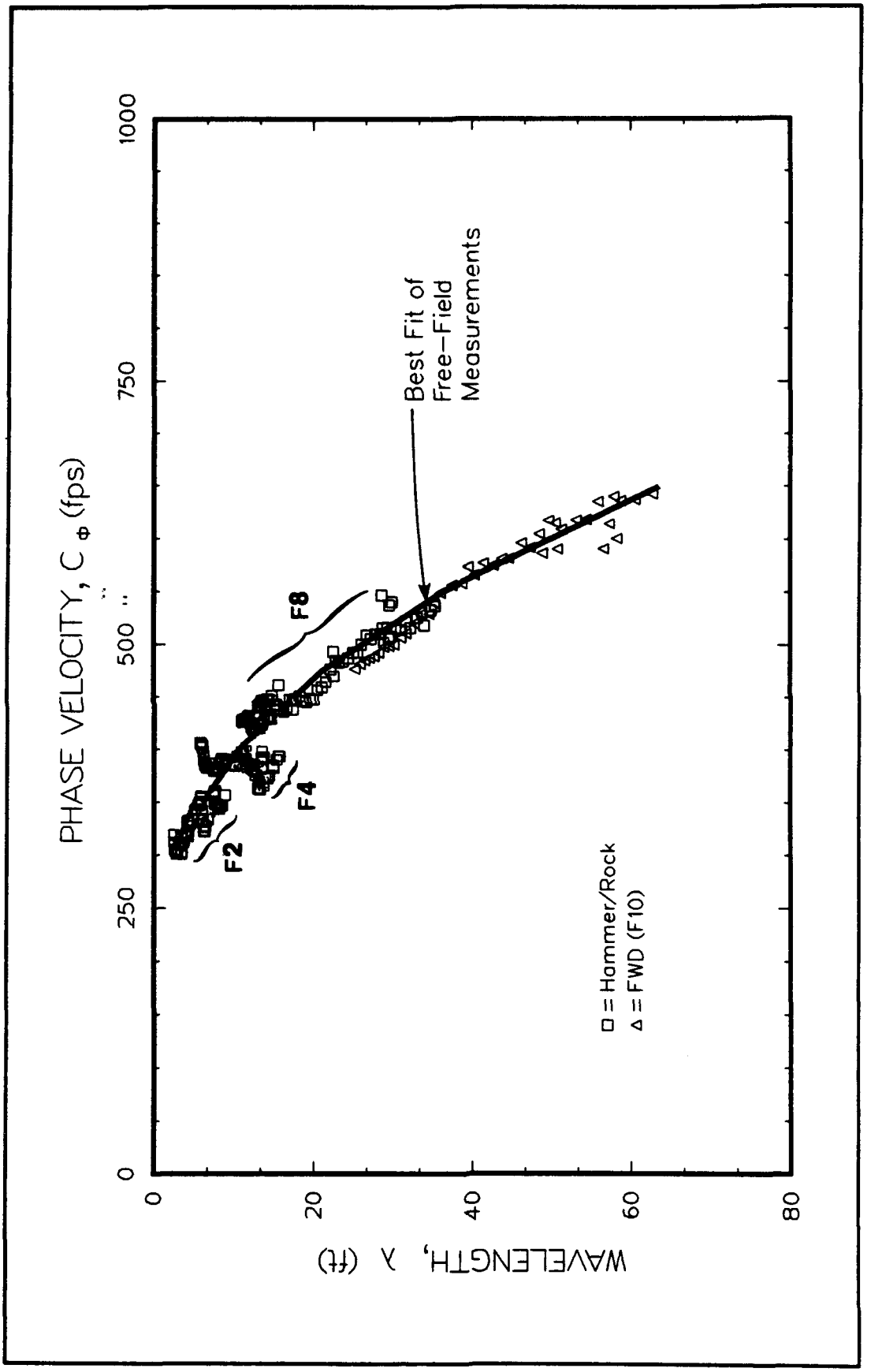

Figure 28. Dispersion curve derived from level ground measurements

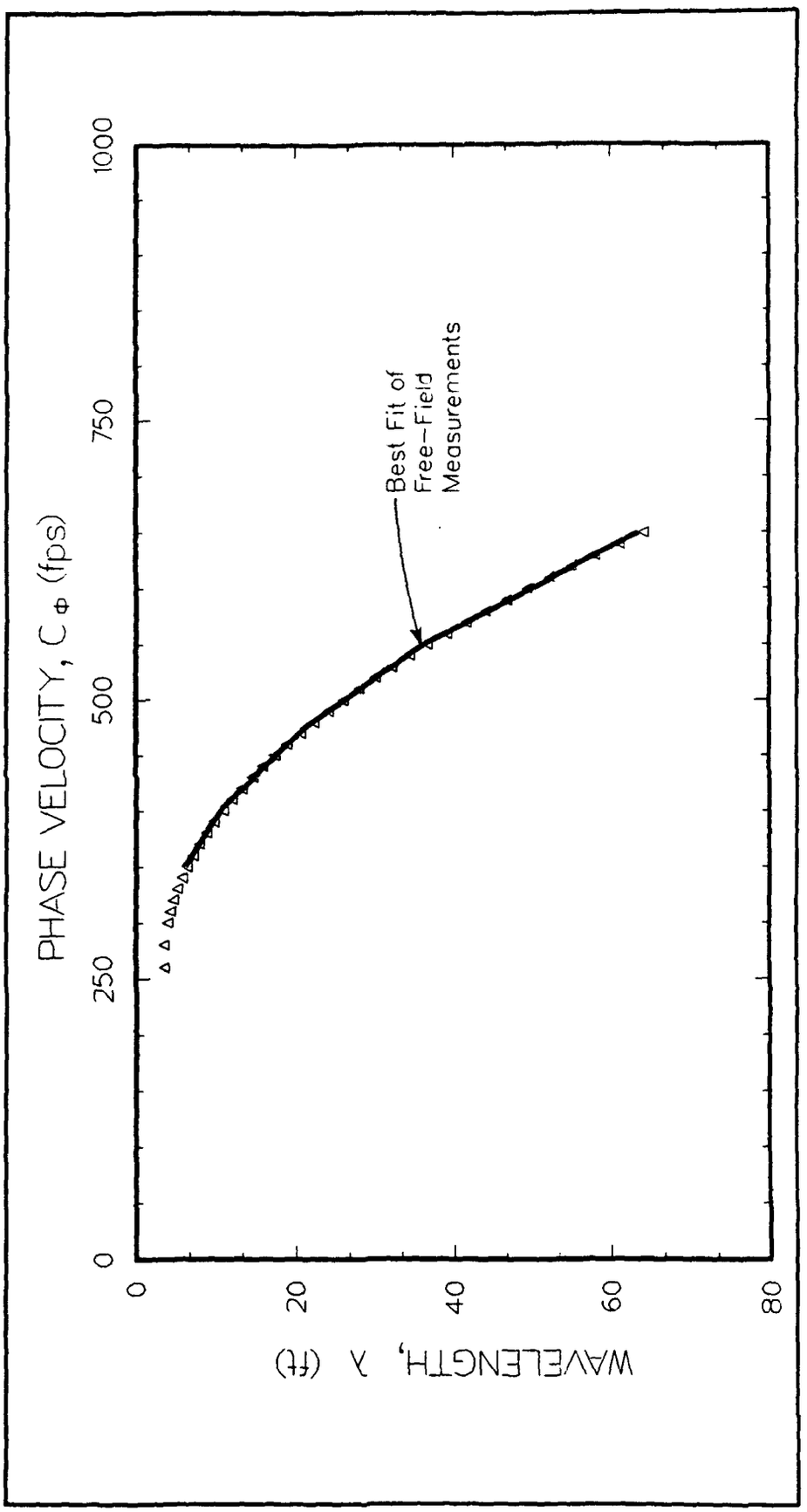

Figure 29. Final iterated dispersion curve in comparison to best fit of level ground measurements

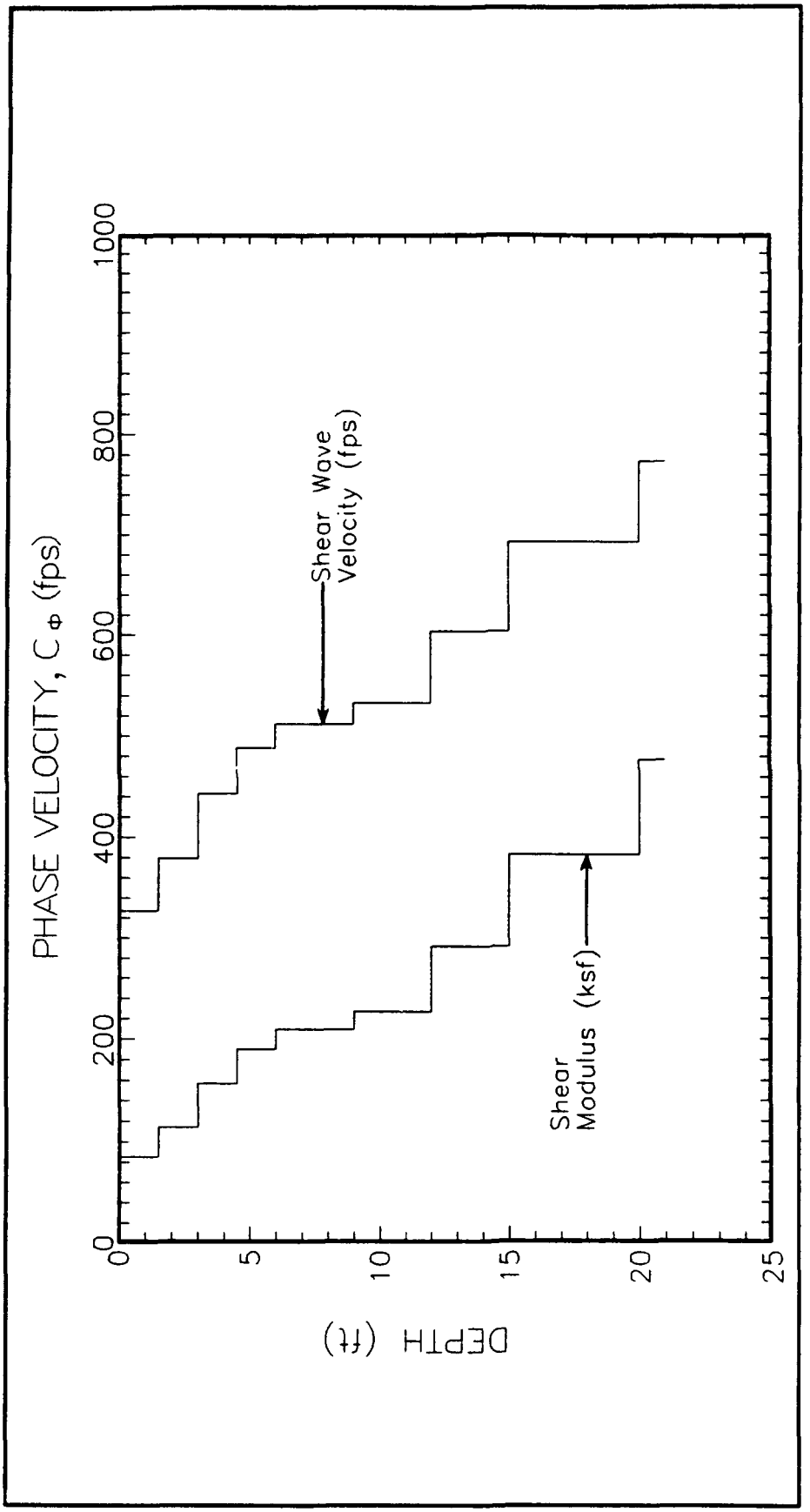

Figure 30. Variation of level ground stiffness derived from final iterated dispersion curve

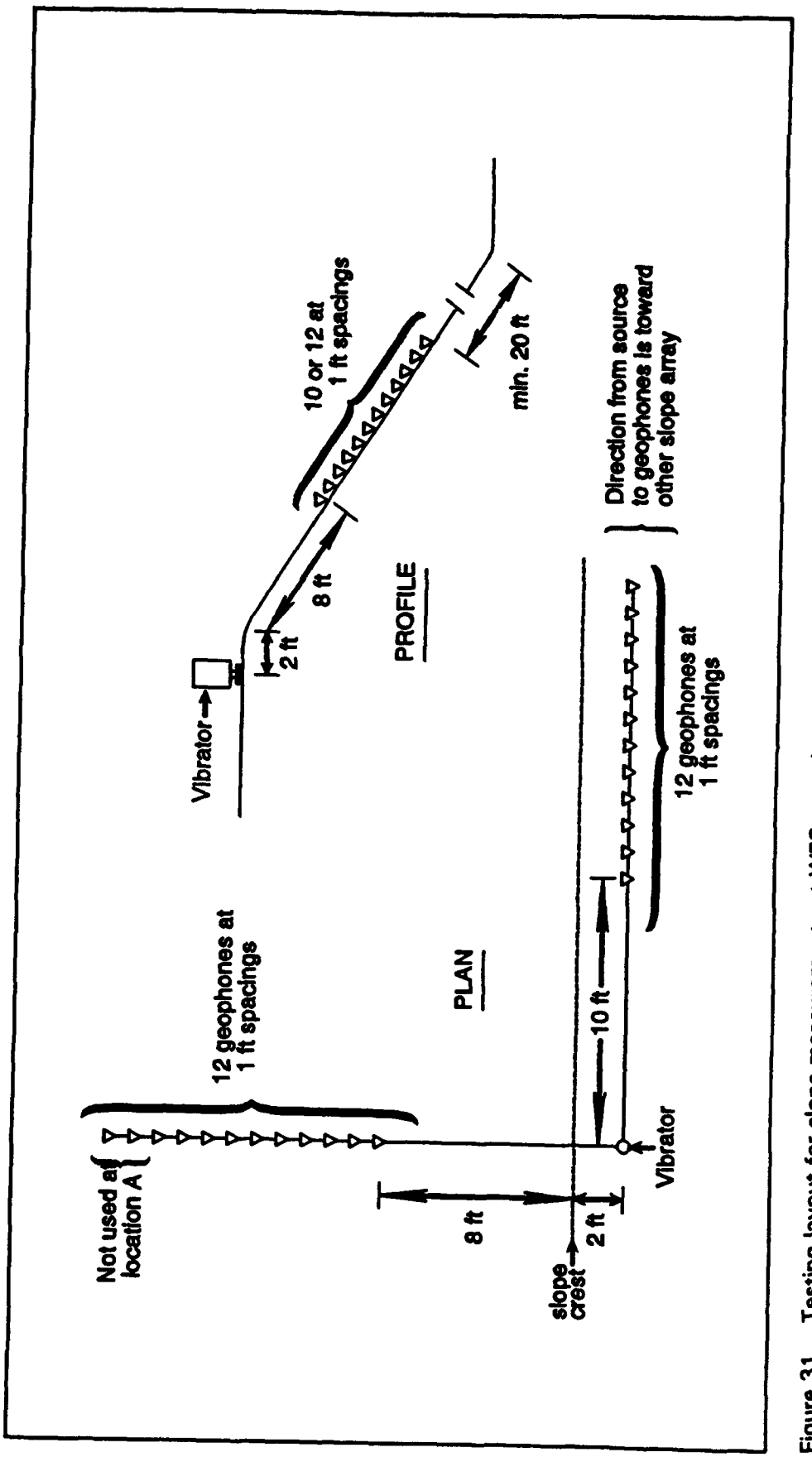

Figure 31. Testing layout for slope measurements at WES test site

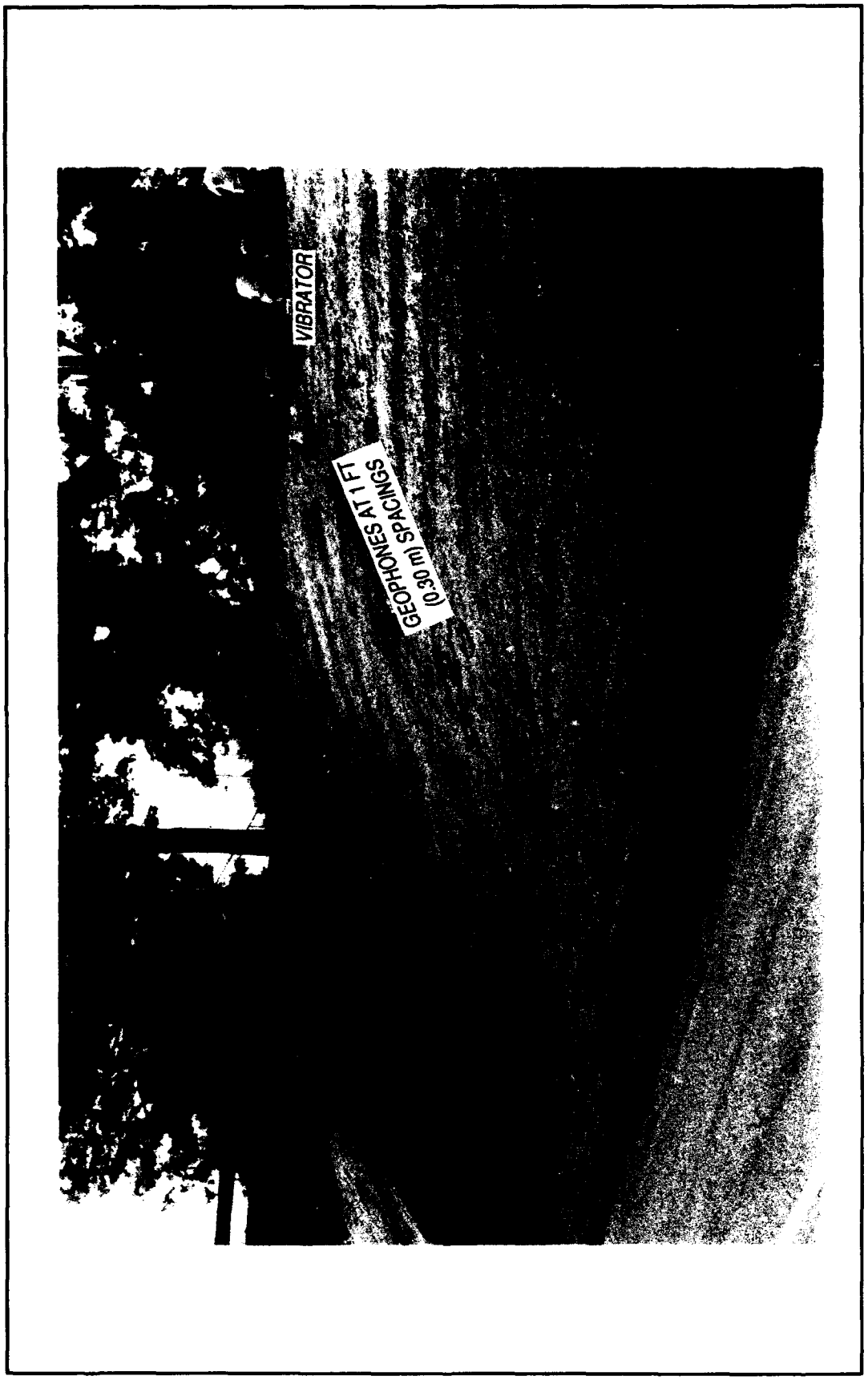

Figure 32. View of test configuration for measurements made downslope looking southeast

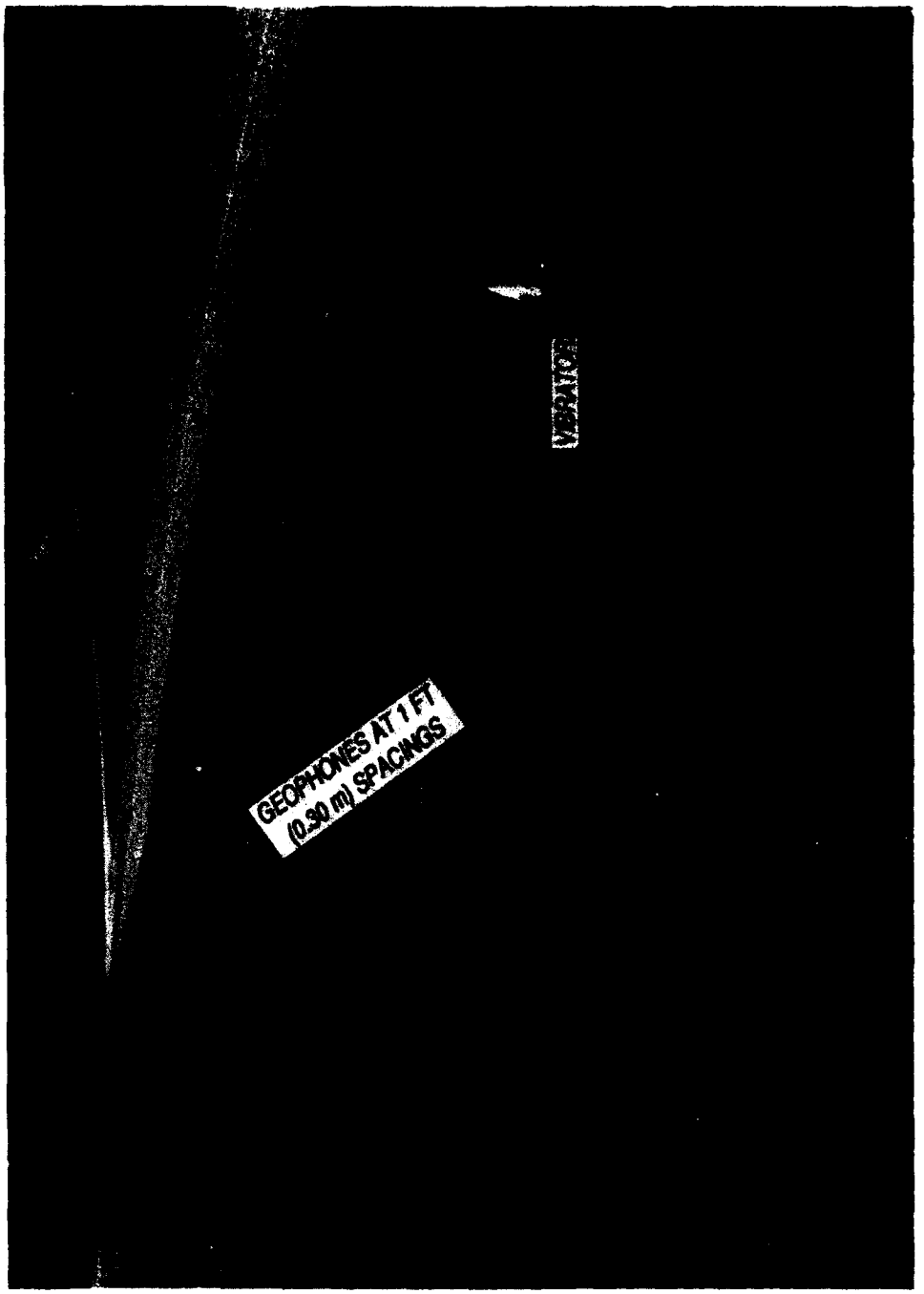

Figure 33. View of test configuration for measurements made along the crest looking northwest

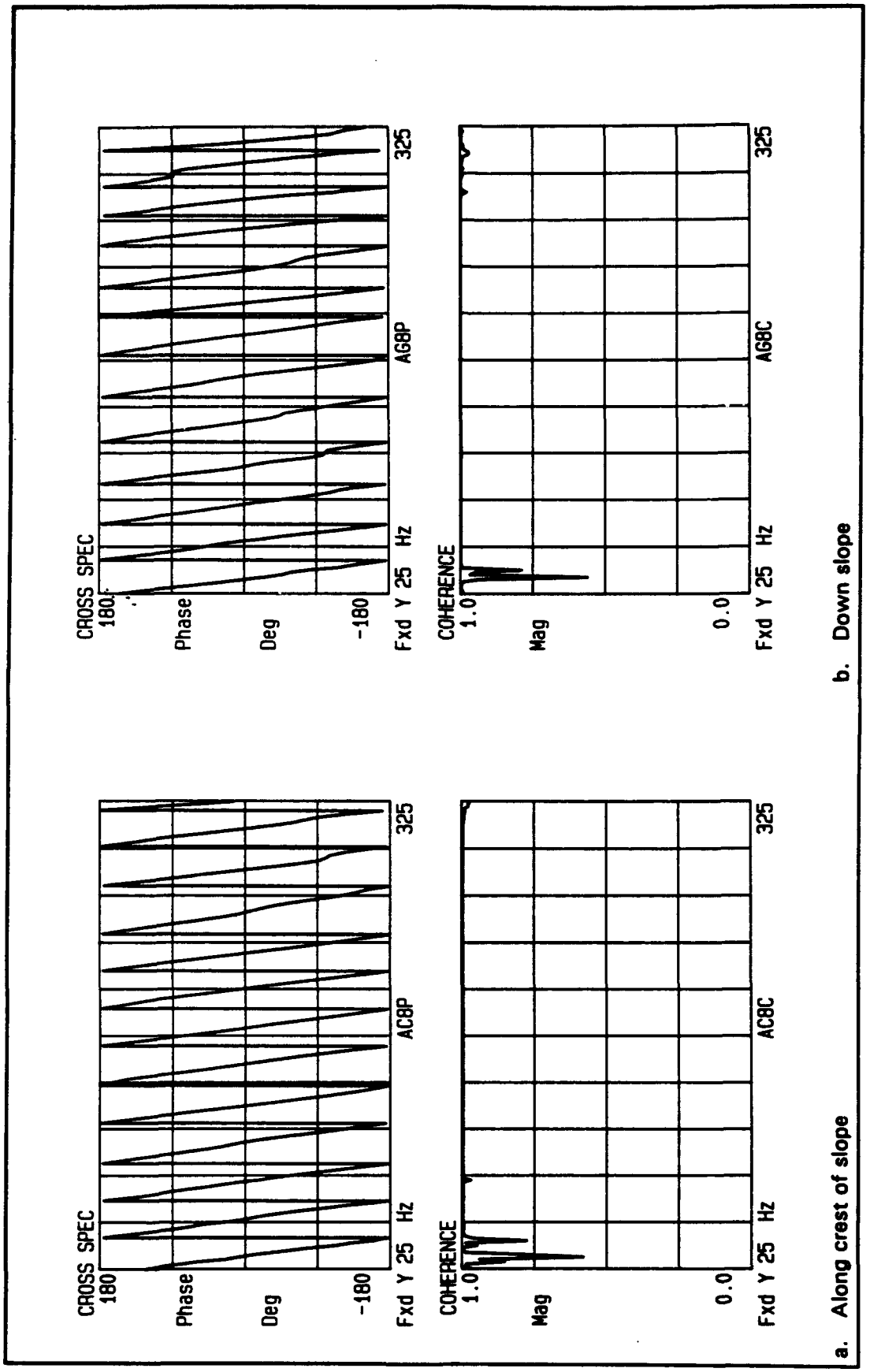

Figure 34. Typical phase difference and coherence between source and receiver for slope measurements and harmonic source

greater than about 125 Hz). These data (both phase and coherence) are much better than that measured at the level ground array (refer to Figure 3).

The FWD was also used as a source for measurements made near the slope but was found to be inferior to the harmonic sources. Both the phase and coherence between the two receivers are very poor and inconsistent as shown in Figure 35. This suggests that impulsive sources may not be appropriate to measure dynamic displacements near slopes.

The measured displacements were examined at a number of discrete frequencies between 50 and 150 Hz. Typical results of slope measurements are shown in Figures 36 and 37. These figures present the real and imaginary parts of measured displacements, wrapped and unwrapped phase for propagation down the slope and along the crest, and the difference between the phase in these two directions.

Comparisons between the real and imaginary parts of displacement (refer to Figures 36a and 37a) show that the magnitudes of displacement are somewhat similar. The distributions of displacement with distance are not very smooth because of the few points used to represent the variation. The amplitude of displacements generally increased as frequency increased but this is attributed to an increase in force output of the vibrator within the range of frequencies swept.

An analysis of the difference in phase created by the slope (refer to Figures 36b and 37b) indicates that a phase lag does occur for the sloping (down) condition. This phase lag appears to be fairly constant as a function of surface distance, especially when d_1 and d_2 are less than 5λ. (At much larger distances, the difference in phases has a constant change with distance.) Variability in the calculated phase difference is attributed to variability in the soil deposit and sensor distances. These findings are consistent with the results of numerical approximations at distances greater than $3\lambda/4$ beyond the discontinuity.

Comparisons were also made in terms of the magnitude of phase velocity between level ground and slope measurements in the form of dispersion curves (wavelength versus frequency and velocity versus depth). Wavelength is determined from the slope of the unwrapped phase relation (versus distance). Phase velocity may then be calculated using Equation 2.7. Wavelength was calculated at every eighth frequency (increments of 3.0 Hz) beginning at 35 Hz and continuing to 179 Hz using a least-squares fit of the unwrapped phase at locations where the coherence between the sources and receiver was greater than 0.99.

The data show that a discontinuity and slope generally do not disperse surface waves. The data, in terms of wavelength versus frequency, are shown in Figure 38 for each slope site and direction. Contours of velocity are also shown along with the best-fit relationship derived from level ground measurements. The wavelengths from the two locations and two directions are very similar except when $f >$ 125 Hz where some scatter is produced for

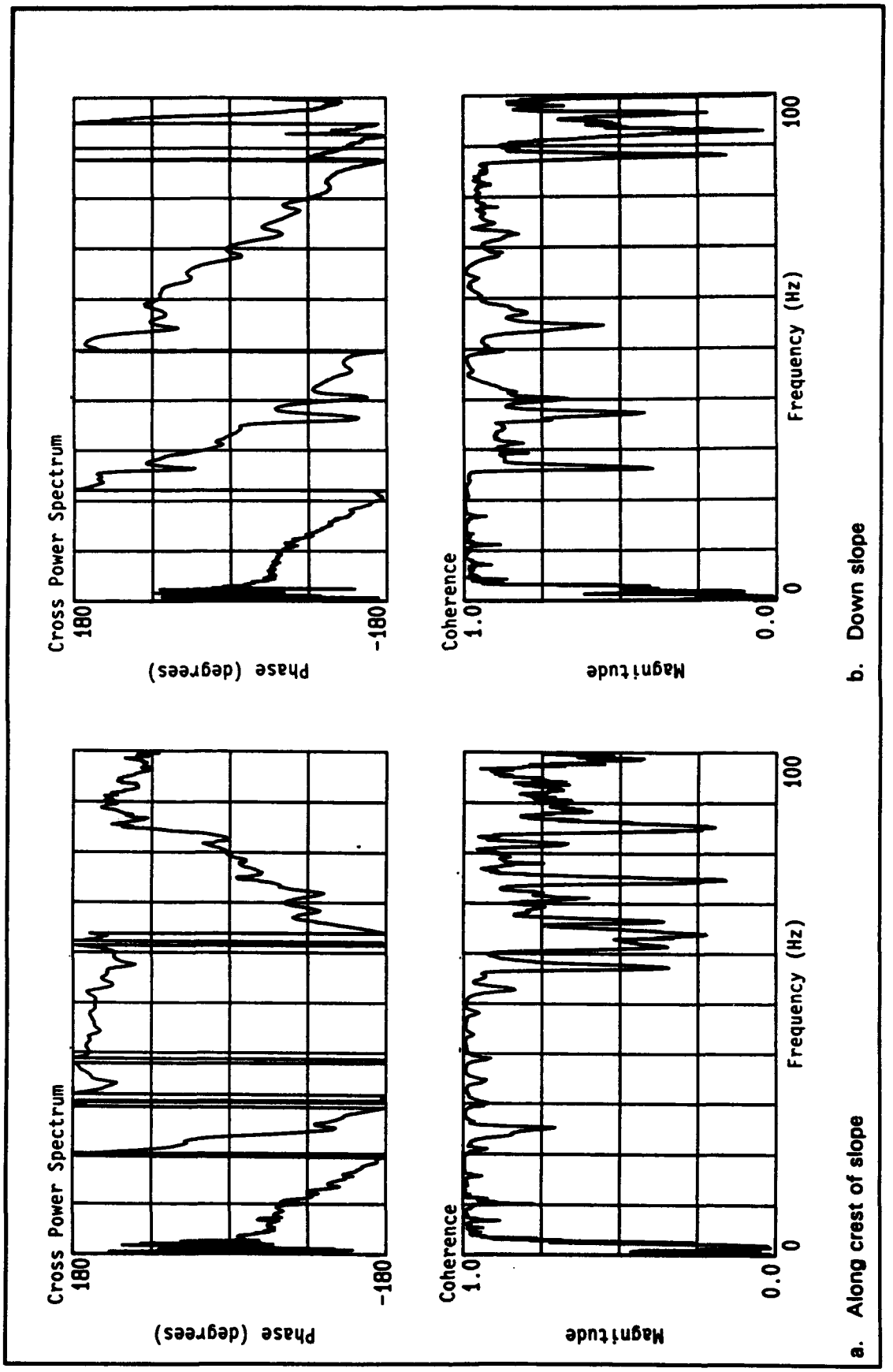

Figure 35. Typical phase difference and coherence between receivers for sloping ground measurements and impulsive sources

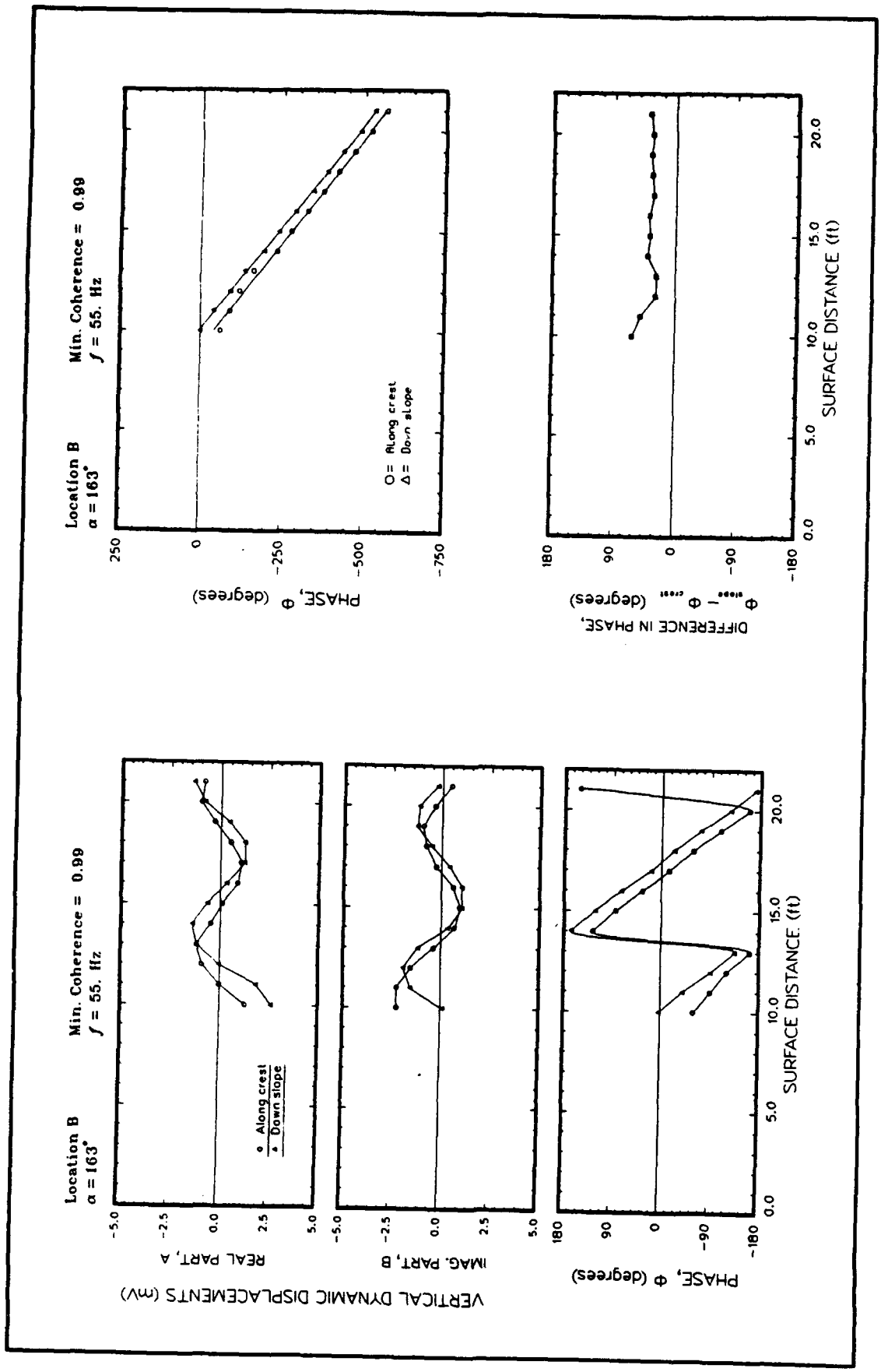

Figure 36. Results for measurements at Location B and frequency of 55 Hz

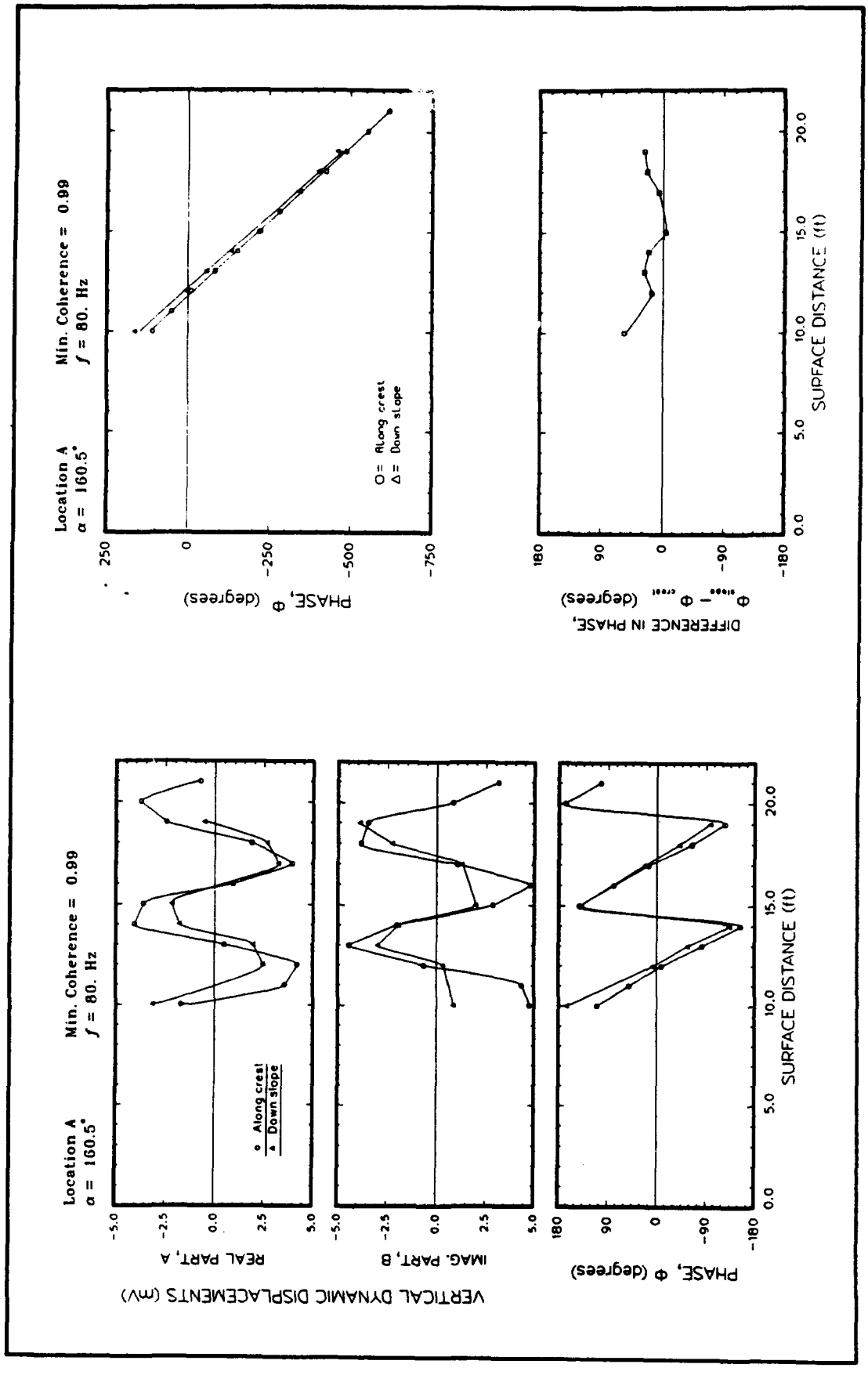

Figure 37. Results for measurements at Location A and frequency of 80 Hz

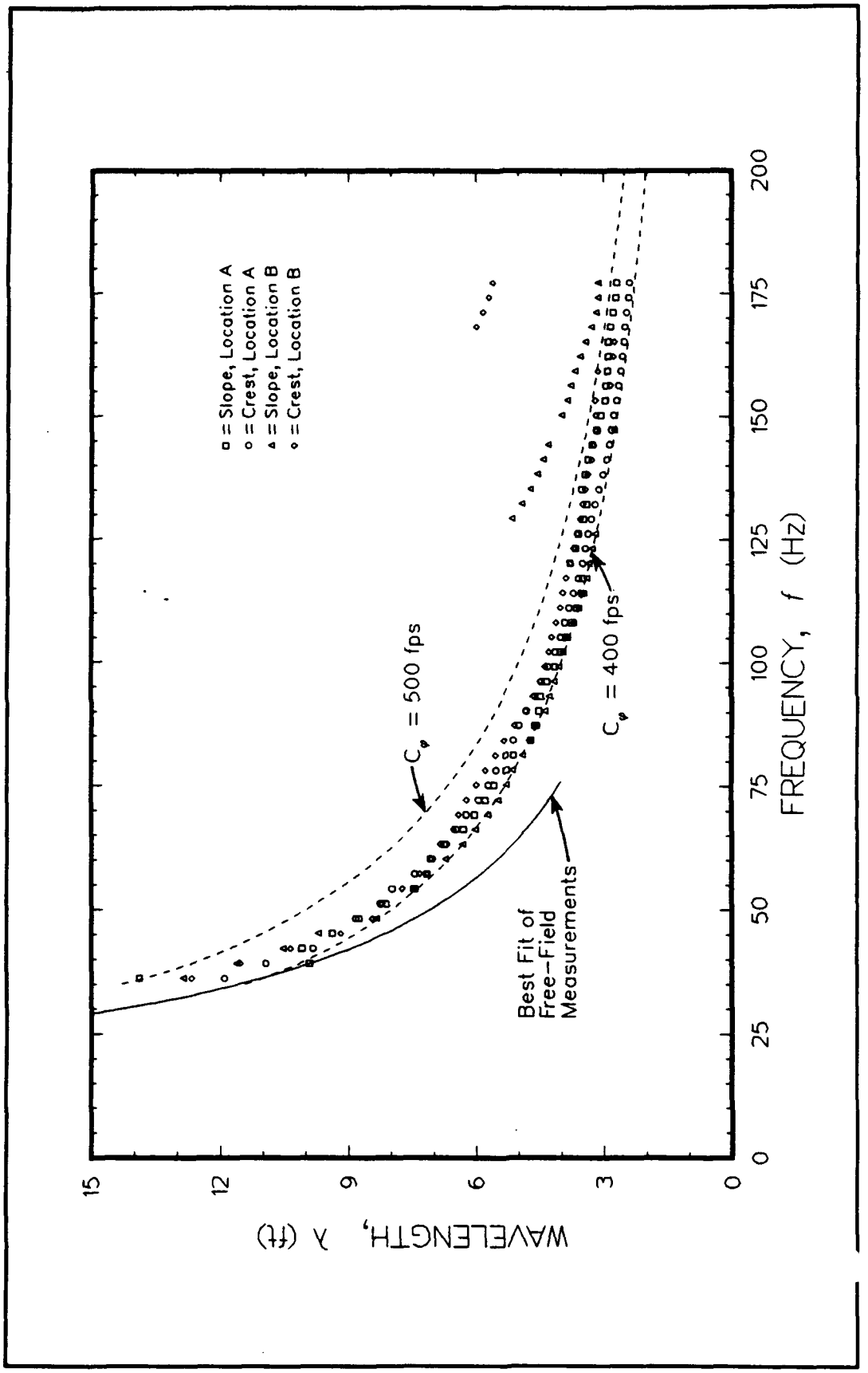

Figure 38. Compilation of results from slope measurements showing range in phase velocities and comparison with level ground measurements

Location B and is attributed to aliasing. The data for $f < 125$ Hz generally fall within a band of phase velocities between 400 and 450 fps and come closer to level ground measurements as λ increases.

The data, in terms of wavelength versus phase velocity (dispersion curve) for $f < 125$ Hz, are shown in Figure 39a along with the best-fit relationship derived from level ground measurements. The average phase change over the length of the array was calculated using a least squares fit algorithm. Average phase relations are shown as straight lines in Figures 29 and 30. These phase velocities tend to fall within a narrow band between 400 and 460 fps but are significantly larger than the best-fit relationship for level ground measurements and begin to deviate more as λ decreases below 9 ft. Phase velocities along the crest are generally greater than phase velocities measured down the slope.

Phase velocities measured in sloping ground were also compared with level ground measurements at a spacing of eight feet. Measured values of phase corresponding to the first and ninth receiver (d_1 = 10 ft and d_2 = 18 ft) were subtracted and the velocity calculated and compared with the best-fit relationship and the 8-foot-spacing data (F4) from the free field as shown in Figure 39b. A close match exists between phase velocities measured in the free field and down the slope although the slope velocities tend to be slightly greater.

The phase velocities may be greater along the crest because of site grading and compaction that probably occurred during development of the area. The effort of field compaction is likely to be greater near the crest and less down the slope which would tend to produce greater velocities near the crest.

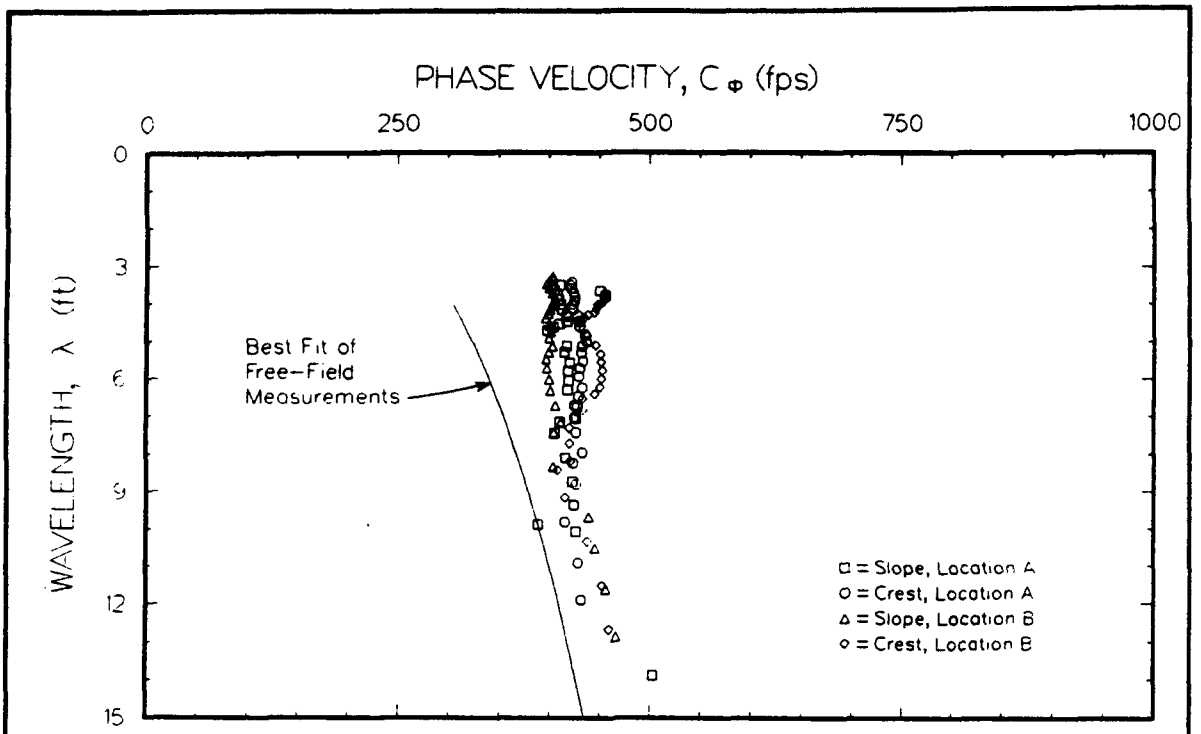

a. Results using least squares fit of all data

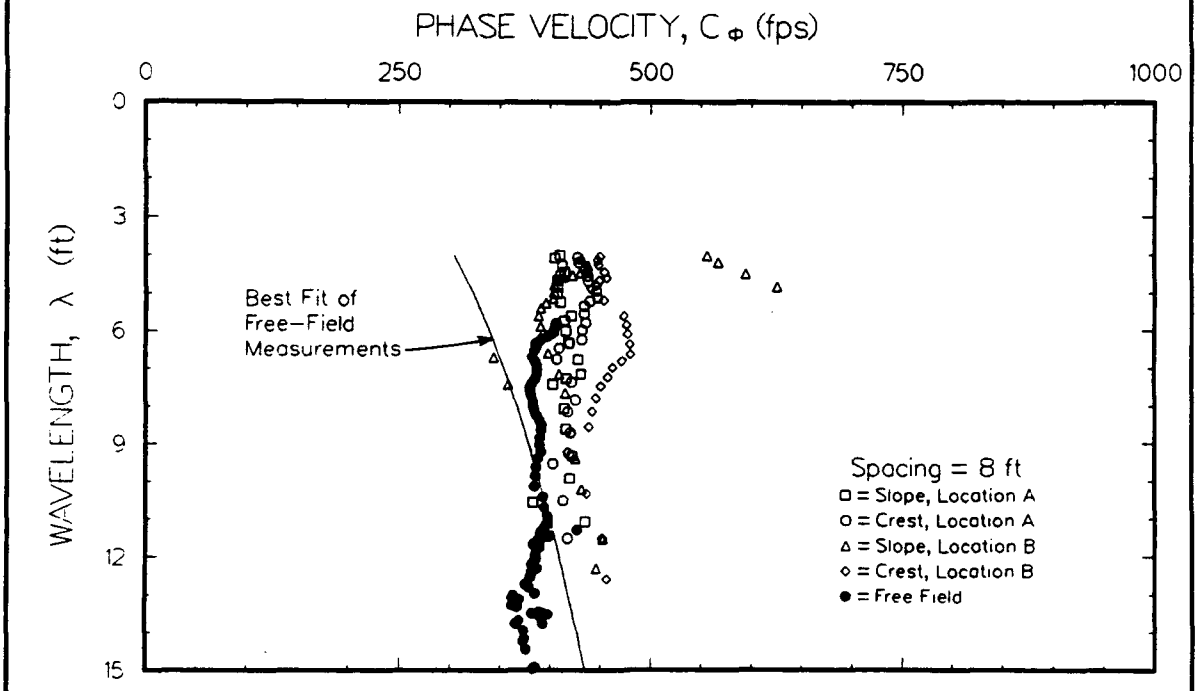

b. Results using 8-ft spacing and d_2/d_1 = 2.3

Figure 39. Dispersion curve from slope measurements and comparison with level ground measurements

6 Summary and Conclusions

The effect of sloping ground on the propagation of surface waves has been examined using a semi-analytical method to calculate dynamic vertical displacements produced by a 3-D harmonic load in planar geosystems. Corroborative measurements of vertical dynamic displacements at a test site on the WES Reservation have also been reported. The results of computations and field measurements suggest that surface wave measurements can be reliably and accurately made at sloping ground sites.

The formulation involves creating a 3-D dynamic stiffness matrix and then condensing the components into an equivalent 2-D dynamic stiffness matrix. The out-of-plane loads are represented by a Fourier expansion and applied as nodal forces. The solution to the system of equations is made for each spatial wavenumber and then the inverse Fourier transform produces the complex dynamic displacements. This method provides very accurate values of static and dynamic displacements. Brief descriptions of the formulation, validation, and parametric analysis have been presented.

The effect of a slope on surface wave propagation is to create a phase shift for waves that intersect the discontinuity. The phase shift is generally positive (phase lag) for sloping down conditions and negative (phase lead) for sloping up conditions. Measurements along the crest and base of the slope are not affected by the presence of the slope. In general, the set-back distance and frequency of excitation were found not to affect measurements in any direction.

Close comparisons were found to exist between the change in phase down the slope and along the crest both in numerical approximations and field measurements conducted at a site at WES. Comparisons were also made between dispersion curves derived from numerical approximations and field measurements. The phase velocities near the slope as calculated using the approximation method tended to be slightly greater than phase velocities measured in the near field. Natural variations in elastic moduli at the test site could easily account for the magnitude of difference that exists. It also appears that harmonic sources may be preferable for measurements in the vicinity of sloping ground.

The assumption of level ground made for inversion schemes does not appear to be a very restrictive limitation. The magnitude of the phase shift

does not need to be known if the receivers are placed sufficiently far away from the edge of the slope. The results are independent of the frequency of excitation and set-back distance given that the load is far enough from the discontinuity.

In conclusion, it appears that non-destructive surface wave measurements, including the current SASW method, can be easily adapted to provide a useful means to obtain material properties in more complex geosystems. Simple relationships may be incorporated into inversion schemes to account for slope discontinuities.

References

Alexander, D. R. (1992). "In Situ Material Characterization for Pavement Evaluation by the Spectral-Analysis-of-Surface Waves (SASW) Method," Technical Report GL-92-10, U.S. Army Engineer Waterways Experiment Station, Vicksburg, MS.

American Association of Transportation Officials. (1991). "Standard Specifications for Seismic Design of Highway Bridges," 15th ed., Washington, DC.

Applied Technology Council. (1981). "Seismic Design Guidelines for Highway Bridges," Publication ATC-6, Redwood City, CA.

Applied Technology Council. (1983). "Seismic Retrofitting Guidelines for Highway Bridges," Publication ATC-6-2, Redwood City, CA.

Ballard, R. F., Jr. (1964). "Determination of Soil Shear Moduli at Depth by In-Situ Vibratory Techniques," Miscellaneous Paper 4-691, U.S. Army Engineer Waterways Experiment Station, Vicksburg, MS.

Calderon, J. D. C. (1985). "Cavity Detection by the SASW Method: Preliminary Studies," Master's Thesis, University of Texas, Austin, TX, 83 pgs.

Fry, Z. B. (1963). "Development and Evaluation of Soil Bearing Capacity, Foundations of Structures," U.S. Army Engineer Waterways Experiment Station, Technical Report 3-362, No. 1, Vicksburg, MS.

Fry, Z. B. (1965). "Dynamic Soils Investigations Project Buggy, Buckboard Mesa Nevada Test Site, Mercury, Nevada," Miscellaneous Paper 4-666, U.S. Army Engineer Waterways Experiment Station, Vicksburg, MS.

Gucunski, N. (1991). "Generation of Low Frequency Rayleigh Waves for the Spectral-Analysis-of-Surface-Waves Method," PhD dissertation, University of Michigan, Ann Arbor, MI.

Hanazato, T., Ugai, K., Mori, M., and Sakaguchi, R. (1991). "Three-Dimensional Analysis of Traffic-Induced Ground Vibrations, *Journal of Geotechnical Engineering*, ASCE, Vol. 117, No. 8, pp 1133-1151.

Hardin, B. O. and Drnevich, V. P. (1972). "Shear Modulus and Damping in Soils: Measurement and Parameter Effects," *Journal of Geotechnical Engineering*, ASCE, Vol. 98, No. 6, pp 603-624.

Haskell, N. A. (1953). "The Dispersion of Surface Waves in Multilayered Media," *Bulletin Seismological Society*, Vol. 43, No. 1, pp 17-34.

Heisey, J. S. (1982). "Determination of In Situ Shear Wave Velocities from Spectral Analysis of Surface Waves," Master's Thesis, University of Texas, Austin, TX, 300 pgs.

Heisey, J. S., Stokoe, K. H. II, and Meyer, A. H. (1982). "Moduli of Pavement Systems from Spectral Analysis of Surface Waves," *Transportation Research Record 852*, Washington, DC, pp 22-31.

Heukelom, W. (1958). "Investigation Into the Dynamic Mechanical Properties of Some Runways in the U.S.A. Carried Out in 1958," Report M-35220, Shell Oil Labs, Amsterdam.

Heukelom, W., and Foster, C. R. (1960). "Dynamic Testing of Pavements," *Journal of Soil Mechanics and Foundations Division*, ASCE, Vol. 86, No. SM1, pp. 1-28.

Hiltunen, D. R. (1988). "Experimental Evaluation of Variables Affecting the Testing of Pavements by the Spectral-Analysis-of-Surface-Waves Method," U.S. Army Engineer Waterways Experiment Station, Technical Report GL-88-12, Vicksburg, MS.

Hudson, J. A. and Knopoff, L. (1964). "Transmission and Reflection of Surface Waves at a Corner: 2. Rayleigh Waves (Theoretical)," *Journal of Geophysical Research*, Vol. 69, No. 2, pp 281-289.

Jones, R. (1958). "In-Situ Measurement of the Dynamic Properties of Soils by Vibration Methods," *Geotechnique*, Vol. 8, pp 1-21.

Johnston, D. H., Toksoz, M. N., and Timur, A. (1979). "Attenuation of Seismic Waves in Dry and Saturated Rocks: II. Mechanisms," *Geophysics*, Vol. 44, pp 691-711.

Kang, Y. V. (1990). "Effect of Finite Width on Dynamic Deflections of Pavements," PhD dissertation, University of Texas, Austin, TX.

Kausel, E. (1981). "Explicit Solution for the Green Functions for Dynamic Loads in Layered Media," MIT Research Report R81-13, Cambridge, MA.

_____. (1989). "**PUNCH**: Program for the Dynamic Analysis of Layered Soils," ver. 3.0, Massachusetts Institute of Technology, Cambridge, MA.

Lai, J. Y. and Booker, J. R. (1991). "Application of Discrete Fourier Series to the Finite Element Stress Analysis of Axi-Symmetric Solids," *Internationl Journal, Numerical Methods Engineering*, Vol. 31, pp 619-647.

Lin, H. T. and Tassoulas, J. L. (1987). "Discrete Green Functions for Layered Strata," *International Journal, Numerical Methods Engineering*, Vol. 24, pp 1645-1658.

Miranda, E. (1993). "Evaluation of Seismic Design Criteria for Highway Bridges," *Earthquake Spectra*, Vol. 9, No. 2, pp 233-250.

Nazarian, S. (1984). "In Situ Determination of Elastic Moduli of Soil Deposits and Pavement Systems by Spectral-Analysis-of-Surface-Waves Method," PhD dissertation, University of Texas, Austin, TX, 452 pgs.

Nazarian, S. and Desai, M. (1993). "Automated Surface Wave Method: Field Testing," *Journal of Geotechnical Engineering*, ASCE, Vol. 119, No. 7, pp 1790-1804.

Nazarian, S. and Stokoe, K. H. II. (1985a). "In Situ Determination of Elastic Moduli of Pavement Systems by Spectral-Analysis-of-Surface-Waves Method (Practical Aspects)," Research Report No. 368-1F, Center Transportation Research, Austin, TX.

_____. (1985b). "In Situ Determination of Elastic Moduli of Pavement Systems by Spectral-Analysis-of-Surface-Waves Method (Theoretical Aspects)," Research Report No. 437-1, Center Transportation Research, Austin, TX.

Nogueira, E. C. (1986). "Effects of Cavities on the Propagation of Surface Waves," Master's Thesis, University of Texas, Austin, TX, 96 pgs.

Rix, G. J. (1988). "Experimental Study of Factors Affecting the Spectral-Analysis-of-Surface-Waves Method," PhD dissertation, University of Texas, Austin, TX, 316 pgs.

Rix, G. J. and Leipski, E. A. (1991). "Accuracy and Resolution of Surface Wave Inversion," *Recent Advances in Instrumentation, Data Acquisition, and Testing in Soil Dynamics*, ASCE, Geotechnical Pub. No. 29, ed. Bhatia and Blaney, pp 17-32.

Runesson, K. and Booker, J. R. (1982). "Efficient Finite Element Analysis of 3D Consolidation," *Numerical Methods Geomechanics*, ed. Eisenstein, Balkema Press, Rotterdam, pp 359-364.

_____. (1983). "Finite Element Analysis of Elastic-Plastic Layered Soil Using Discrete Fourier Series Expansion," *International Journal, Numerical Methods Engineering*, Vol. 19, pp 473-478.

Sanchez-Salinero, I. (1987). "Analytical Investigation of Seismic Methods Used for Engineering Applications," PhD dissertation, University of Texas, Austin, TX, 402 pgs.

Sheu, J. C. (1987). "Applications and Limitations of the Spectral-Analysis-of-Surface-Waves Method," PhD dissertation, University of Texas, Austin, TX.

Sykora, D. W. (1993). "Dynamic Vertical Displacements in Planar Geosystems," PhD dissertation, University of Texas, Austin, TX, 237 pgs.

Sykora, D. W. and Roesset, J. M. (1992). "2-D Planar Geosystems Subjected to 3-D Dynamic Loads," Technical Report GL-92-16, U.S. Army Engineer Waterways Experiment Station, Vicksburg, MS, 191 pgs.

Thomson, W. T. (1950). "Transmission of Elastic Waves Through a Stratified Solid Medium," *Journal Sound Vib.*, Vol. 2, No. 3, pp 210-226.

Toksoz, M. N., Johnston, D. H., and Timur, A. (1979). "Attenuation of Seismic Waves in Dry and Saturated Rocks: II. Laboratory Measurements," *Geophysics*, Vol. 44, pp 681-690.

Winnicki, L. A. and Zienkiewicz, O. C. (1979). "Plastic (or Visco-Plastic) Behaviour of Axisymmetric Bodies Subjected to Non-Symmetric Loading for Semi-Analytical Finite Element Solutions," *International Journal, Numerical Methods Engineering*, Vol. 14, pp 1399-1412.

Wolf, J. P. (1985). *Dynamic Soil-Structure Interaction*, Prentice-Hall, Inc., Englewood Cliffs, NJ, pp 15-16.

REPORT DOCUMENTATION PAGE

Form Approved
OMB No. 0704-0188

1. AGENCY USE ONLY (Leave blank)	2. REPORT DATE	3. REPORT TYPE AND DATES COVERED
	April 1994	Report 1 of a series

4. TITLE AND SUBTITLE

Determination of Soil Moduli in Soil-Structure Systems on Highways; Report 1: Surface Waves in Sloping Ground

5. FUNDING NUMBERS

6. AUTHOR(S)

David W. Sykora, Don R. Alexander, Jose M. Roesset

7. PERFORMING ORGANIZATION NAME(S) AND ADDRESS(ES)

U.S. Army Engineer Waterways Experiment Station
3909 Halls Ferry Road, Vicksburg, MS 39180-6199;
Dept. of Civil Engineering, University of Texas,
Austin, TX 78712

8. PERFORMING ORGANIZATION REPORT NUMBER

Technical Report GL-94-11

9. SPONSORING/MONITORING AGENCY NAME(S) AND ADDRESS(ES)

U.S. Army Corps of Engineers
Washington, DC 20314-1000

10. SPONSORING/MONITORING AGENCY REPORT NUMBER

11. SUPPLEMENTARY NOTES

Available from National Technical Information Service, 5285 Port Royal Road, Springfield, VA 22161.

12a. DISTRIBUTION/AVAILABILITY STATEMENT

Approved for public release; distribution is unlimited.

12b. DISTRIBUTION CODE

13. ABSTRACT *(Maximum 200 words)*

Data collection and processing methods for most seismic geophysical methods used to characterize engineering sites assume that the ground surface is level and that the sub-surface layers are horizontal and extend to infinity. These assumptions do not apply to some highway sites which exist on embankments or at bridge abutments or foundations.

The objectives of the overall program are to examine the effects of complex geosystems (soil-rock-structure) and anisotrophic states of stress on existing databases, and develop best field system to derive elastic moduli in embankments and obtain effective dynamic earth pressures.

This report summarizes the results of numerical approximations using a new research tool and field measurements to evaluate the effect of sloping ground on the Spectral-Analysis-of-Surface-Waves (SASW) method. The combined results suggest that surface wave measurements can be reliably and accurately made at sloping ground sites with little modification to existing measurement techniques.

14. SUBJECT TERMS

Numerical modeling
Seismic geophysics
Site characterization
Vibration
Wave propagation

15. NUMBER OF PAGES

64

16. PRICE CODE

17. SECURITY CLASSIFICATION OF REPORT	18. SECURITY CLASSIFICATION OF THIS PAGE	19. SECURITY CLASSIFICATION OF ABSTRACT	20. LIMITATION OF ABSTRACT
UNCLASSIFIED	UNCLASSIFIED		